

A deeper look at the colors of the Saturnian irregular satellites

Tommy Grav

Harvard-Smithsonian Center for Astrophysics,
MS51, 60 Garden St., Cambridge, MA02138

and

Institute for Astronomy, University of Hawaii,
2680 Woodlawn Dr., Honolulu, HI86822

tgrav@cfa.harvard.edu

James Bauer

Jet Propulsion Laboratory, California Institute of Technology
4800 Oak Grove Dr., MS183-501, Pasadena, CA91109

bauer@scn.jpl.nasa.gov

September 13, 2018

Manuscript: 36 pages, with 11 figures and 5 tables.

arXiv:astro-ph/0611590v2 8 Mar 2007

Proposed running head: Colors of Saturnian irregular satellites

Corresponding author:

Tommy Grav
MS51, 60 Garden St.
Cambridge, MA02138
USA
Phone: (617) 384-7689
Fax: (617) 495-7093
Email: tgrav@cfa.harvard.edu

Abstract

We have performed broadband color photometry of the twelve brightest irregular satellites of Saturn with the goal of understanding their surface composition, as well as their physical relationship. We find that the satellites have a wide variety of different surface colors, from the negative spectral slopes of the two retrograde satellites S IX Phoebe ($S' = -2.5 \pm 0.4$) and S XXV Mundilfari ($S' = -5.0 \pm 1.9$) to the fairly red slope of S XXII Ijiraq ($S' = 19.5 \pm 0.9$). We further find that there exist a correlation between dynamical families and spectral slope, with the prograde clusters, the Gallic and Inuit, showing tight clustering in colors among most of their members. The retrograde objects are dynamically and physically more dispersed, but some internal structure is apparent.

Keywords: Irregular satellites; Photometry, Satellites, Surfaces; Saturn, Satellites.

1 Introduction

The satellites of Saturn can be divided into two distinct groups, the regular and irregular, based on their orbital characteristics. The regular satellites are believed to have been created in a scenario similar to the Solar System, accreting out of a circumplanetary disk of gas and dust. They are thus on prograde, nearly circular orbits close to the equatorial plane of their host planet. The irregular satellites are thought to be captured heliocentric objects, but their origin or capturing processes are not well understood.

The first irregular satellite of Saturn was S IX Phoebe, discovered by W. Pickering in 1898. It would not be until a full century later that the next irregular satellite of Saturn was announced, when Gladman *et al.* (2001) reported their discovery of 12 new irregular satellites, ranging in size from 5 to 35 km in diameter. Subsequent surveys by Sheppard *et al.* (2003, 2006) and Jewitt *et al.* (2005) have raised the number of known Saturnian irregular satellites to a total of 35.

The irregular satellites of Saturn were recognized to be clustering in orbital elements by Gladman *et al.* (2001). They suggested that the clustering was due to the breakup of several larger progenitors, similar to the creation of the asteroidal families. The Saturnian irregular satellites seem to make up two clear prograde families, named after Inuit and Gallic gods respectively, and a much more dispersed retrograde group, named after the Norse ice giants. It is not clear whether these retrogrades are fragments of one or more captured progenitors, although the great dispersion of the 18 known retrograde satellites makes the idea of several progenitors more likely. To test the hypothesis that the dynamical families are indeed fragments of larger progenitors Grav *et al.* (2003) presented *BVRI* photometry of 8 saturnian irregular satellites. The prograde families were indeed found to have homogeneous colors, but only 3 of the objects had $1\text{-}\sigma$ uncertainty less than 0.05 across all color, making it hard to strongly argue in favor of the hypothesis proposed by Gladman *et al.* (2001).

In order to place constraints on the many capturing mechanisms that have been proposed to cause the creation of the irregular satellite population, it is necessary to understand the number of events needed to create the currently observed dynamical structure. Irregular satellites are generally considered to have been captured by their host planets from heliocentric orbits Gladman *et al.* (2001). Due to the time reversibility of the pure gravitational three-body capture (sun-planet-satellite) the object is only temporarily in orbit around the planet unless some dissipative mechanism exist to make the capture permanent. At least five different processes have been proposed: 1) capture due to collisions between a temporarily captured object and an existing satellite, or between two temporarily captured objects (Colombo and Franklin, 1971; Gladman *et al.*, 2001); 2) capture due to a mass increase in the host planet (Heppenheimer and Porco, 1977); 3) capture due to gas drag from a gas envelope or gas disk around the planet (Pollack *et al.*, 1979; Ćuk and Burns, 2004a); 4) capture through three-body interaction with other temporarily captured objects (Jewitt and Sheppard, 2005); 5) capture during planetary resonance passage (Ćuk and Gladman, 2006). It is evident that a better understanding of the physical and dynamical structure of the irregular satellites, as well as determining the number of capturing events, is essential in constraining and potentially eliminating some of these proposed mechanisms. Note that it is still not clear whether one mechanism dominates the capture, or whether the irregular satellites observed today are the result of capture through several of the proposed mechanisms.

The study of the physical characteristics of the irregular satellites is also an integral part in determining the origins of the progenitors. Understanding where the irregular satellites originate from and how they reached the phase space of the giant planets is essential in order to improve our understanding of the transfer of matter within the early Solar System. Several origins have been proposed for the irregular satellites. Ćuk and Burns (2004a) proposed that the Himalia family

originated among the Hilda asteroids in the outer main asteroid belt. The recent flyby of S IX Phoebe by the Cassini spacecraft just 19 days before orbital insertion into the Saturnian system provided a wealth of new information. Johnson and Lunine (2005) argued that the measured density of Phoebe, at $\rho \sim 1630 \pm 45 \text{kgm}^{-3}$, indicates that Phoebe has its origin in the outer Solar System. Origins among the trojan population and local population of planetesimals at the later stages of giant planet formation has also been proposed.

This paper presents optical photometry collected using the GMOS-N imager on the 8m Gemini North telescope and the LRIS-R&B imager on the the 10m Keck I telescope in preparation for thermal observations of the irregular satellites with the MIPS instrument on the Spitzer Space Telescope. It also provides an errata to a measurement of Albiorix published in Grav *et al.* (2003).

2 Observations

Optical photometry of 7 Saturnian irregular satellites in the g' , r' , i' and z' SDSS-filters were collected through queue observations on November 9th and 10th, 2004 and classical observing on April 13th and 15th, 2005, both using the Gemini Multi-Object Spectrograph North (GMOS-N) instrument at the 8-m Gemini Observatory on Mauna Kea, Hawaii. GMOS-N has a ~ 5 by ~ 5 arcmin field of view, with 0.073 arcsec per pixel. All observations with this instrument were done in binned mode (0.146 arcsec per pixel), which with seeing in the range 0.75 – 1 arcsec gave excellent sampling of the point spread function of our targets. Optical photometry of 8 Saturnian satellites were also collected in the Johnson-Kron-Cousins BVRI filters on January 6th, 2005, using the Low Resolution Imaging Spectrometer (LRIS) on the 10m Keck I telescope, also located on Mauna Kea, Hawaii. LRIS has two detectors, the red and blue side of the instrument, allowing observations in two filters simultaneous. The red side has a field of view of ~ 7 by ~ 7 arcmin, with a plate scale of 0.21 arcsec per pixel. The blue side has field of view of ~ 9 by ~ 9 arcmin, with a plate scale of 0.135 arcsec per pixels. In addition we report the re-reduction of one observation from the Grav *et al.* (2003) that was found to be erroneous. The observational circumstances are given in Table 1.

The data were collected by observing each object in a RBBRVRIIR sequence (or the equivalent for the SDSS filter set), to make sure that rotational light curve effects did not influence the computed colors. All images were taken with sidereal tracking and the exposure time was kept short enough to avoid trailing of the satellites. Images in each of the filters were then combined to increased the signal-to-noise ratio of the science targets.

The collected data was reduced using aperture corrected photometry with the IRAF/DAOPHOT package (Tody, 1993; Davis, 1994). Science target aperture radii were selected at $\sim 1.3 \times \text{fwhm}$ and aperture correction values were determined using outer aperture radii of $3 - 4 \times \text{fwhm}$ on $\sim 8 - 12$ field stars. Background flux were calculated using an aperture radius from ~ 4 to ~ 8 times the full-width-half-max (fwhm) of the fields point spread function (psf). Zero point magnitudes, airmass and color corrections were determined using a set of Landolt (1992) standard stars taken on the same nights as the science observations. In order to compare the resulting photometry the SDSS filtered observations were converted to the BVRI filter system. Transformation equations between the SDSS photometric system ($g'r'i'z'$) and the standard Johnson-Kron-Cousins system (Johnson and Morgan, 1953; Cousins, 1978) are given in Fukugita *et al.* (1996) and Jordi *et al.* (2006).

3 Results

With this survey we have performed accurate color broadband photometry of the 12 most luminous Saturnian irregular satellites. We have observed all but one of the prograde satellites (S/2004 S11 in the Gallic family was not observed) and 1/5 of the known retrograde satellites of Saturn. This survey thus constitutes the most comprehensive study of color photometry of the irregular satellites to date. The results are given in Table 2 and show that the colors and spectral slopes of the Saturnian irregular satellites are consistent with C-, D- and P-type asteroids. Solar colors were adopted as $B - V = 0.67$, $V - R = 0.36$ and $V - I = 0.71$ (Hartmann *et al.*, 1982, 1990; Hardorp, 1980; Jewitt and Luu, 1998).

The colors were converted to reflectance and the resulting broadband spectra are given in Fig. 4, 5 and 6 for the Gallic, Inuit and retrograde clusters, respectively. The spectral slope, S'_1 [%per100nm], of the broadband colors are given by

$$S'_1 = \frac{2(10^{0.4(C-C_{sun})} - 1)}{\Delta\lambda(10^{0.4(C-C_{sun})} + 1)} \quad (1)$$

where C and C_{sun} are the colors of the object and sun, respectively. $\Delta\lambda$ is the wavelength difference between the two filters that make up the color (Luu and Jewitt, 1996). The value given for S'_1 in Table 3 are found using the $B - I$ colors of the objects and the sun. Since some of the satellites have apparent non-linear features, we also fitted the four reflectances to a linear slope S'_2 using a linear regression method. Note that for the non-linear slopes of S XXIII Suttungr and S XXX Thrymr the fit was done excluding the V filter reflectance. Fitting the S'_2 gave similar values to the S'_1 calculation. However, S'_2 is generally a better way to derive an average slope solution when the normalized reflectance's deviate significantly from a linear solution, as it uses all four points (or in some cases three points) rather than the two used in calculating S'_1 .

To capture the non-linearity we also fit linear slopes for filter subsets, the BVR filters, $S'_{2(B-R)}$, and for the RI filters, $S'_{2(R-I)}$. All four values for the spectral slope is given in Table 3. Using the spectral slope to taxonomy class values given in Dahlgren and Lagerkvist (1995), we define taxonomy classes for our objects (again see Table 3). It should be noted that the spectral slopes used in Dahlgren and Lagerkvist (1995) are based on the spectral slope in the range 400 – 740nm, while our slopes span the range 430 – 900nm. Since most of the slopes are near linear, we can still safely use the literature values for comparison. The results are plotted in Fig. 7 and show that the Saturnian irregular satellites contain a more or less equal fraction of C-, P- and D-like objects. One object, Ijiraq, has a spectrum that is marginally redder than the D-type objects and we define this as an "medium red"-type object (MR-type; $15\% < S'_2 < 25\%$). No objects appears to have the ultra-red matter (UR-type, $S'_2 > 25\%$) found in the trans-neptunian population (e.q. Jewitt, 2002).

We also look for evidence for the weak absorption feature near $0.7\mu\text{m}$ that has been attributed to an $\text{Fe}^{2+} \rightarrow \text{Fe}^{3+}$. This feature has been shown to appear in spatially resolved spectra (Jarvis *et al.*, 2000b) and in $\sim 50\%$ of the main-belt C-type asteroids through both reflectance spectra and photometry (Vilas, 1994; Bus and Binzel, 2002; Carvano *et al.*, 2003). Using data from 27 low-albedo asteroids, Vilas (1994) showed that there were a $\sim 85\%$ correlation between the $0.7\mu\text{m}$ and the $3.0\mu\text{m}$ spectral feature due to water hydration. The weighted mean values of the $0.7\mu\text{m}$ test for all available observations are given in Table 4.

The observed magnitudes were reduced to absolute magnitudes using the H-G formulation

$$H(1, 1, 0) = m_V - 5 \log(r\Delta) + 2.5 \log((1 - G)\Phi_1(\alpha) + G\Phi_2(\alpha)) \quad (2)$$

where the first correction term is the distance modulus, with r and Δ representing the object's distance in AU from the Sun and observer, respectively, and the second correction term is the phase

modulus (for a more thorough description see *Bowell et al.*, 1989). Using the available observations (both from this paper and literature in general) of the saturnian irregular satellites we fit $H(1, 1, 0)$ and G using a Levenberg-Marquardt least square method. These values are given in Table 4 and the fits are plotted in Fig. 8 to 10. Note that use of photometry reported to the Minor Planet Center (MPC) is generally discouraged for any serious application as it is generally unreliable and no information on the actual filters used is available. However, the MPC photometry used in this paper to derive phase curve parameters are well known to the authors, as they are all from survey and follow-up programs in which the authors are members (*Gladman et al.*, 2001). These observations have a signal to noise ratio of ~ 4 in most cases, thus we assume that the error in the MPC collected photometry is 0.25 magnitudes. It should be noted that several of the less observed objects still have very poor solutions and additional photometric observations are still badly needed to better constrain and utilize the phase curve as a marker for relationships between the irregular satellites of Saturn. However, using the fitted value for the absolute magnitude and assuming an albedo of $p_R = 0.08$ (the average albedo of Phoebe; *Simonelli et al.*, 1999) we calculate the approximate diameter of the saturnian irregular satellites observed in this paper (see Table 4). It should also be noted that without knowledge about the rotational light curve caution should be taken in reading too much into the phase curve parameter. For example, data collected by the authors do show that Ymir has a large rotational light curve amplitude (~ 0.3 peak-to-peak magnitudes) and, while the phase curve fit does not show much scatter around the fit, care is needed when interpreting the result. It should be noted that arguments about the inadequacy of the H-G formulation in detecting the opposition surge for very small phase angles has been made, and several other groups prefer the use of a combination of a linear and exponential function with four free parameters (*Belskaya et al.*, 2006; *Kaasalainen et al.*, 2003). With additional observations such models could be used to better model the apparent strong opposition surge of Paaliaq and Ymir (see Figure 9 and 10, but with the sparse photometry currently available the 2 free parameter of the H-G formulation remains an adequate method for determination of the phase light curve).

In order to study the collisional events as a possible mechanism behind the creation of the apparent dynamical family structure, we used the Gauss equations to calculate the dispersion velocity needed to move the orbits of the fragments from that of the progenitor (*Nesvorný et al.*, 2003, 2004; *Grav et al.*, 2003). We further use the same method as *Nesvorný et al.* (2004) to compute the size of the impactor needed to create such a dispersion velocity assuming that 10% of the impact energy is deposited into the fragments as kinetic energy. Using the derived sizes from Table 4 and an assumed density of $\rho = 1.6 \text{ g/cm}^3$ (*Johnson and Lunine*, 2005) for all bodies we can determine a likely scenario for the collision and fragmentation. Since the collision rates among the satellites or with cometary objects are too low to explain the apparent family structures (*Nesvorný et al.*, 2004), we use remnant planetesimals from early epochs of the Solar System in an attempt to determine the disk mass needed to create the families. We use the same three size distributions as *Nesvorný et al.* (2004), and note that the size distribution based on studies of the in situ formation of the Kuiper belt (*Stern*, 1995; *Kenyon and Luu*, 1998; *Kenyon*, 2002) is an unlikely analog to a disk of remnant planetesimals at Saturn. *Nesvorný et al.* (2004) showed that this distribution (called C in their work) would catastrophically disrupt even the smallest of the known Saturnian irregular satellites, unless the disk have a mass $M_{\text{disk}} \lesssim 10M_{\oplus}$.

3.1 The Gallic Family

This dynamical group is centered around 37° inclination and currently four members are known (see Table 5). Their semi-major axes are also tightly clustered, $a_{\text{avg}} = 207 - 302$ saturn radii (R_S),

compared to the large spread among all the known Saturnian satellites, $a_{\text{avg}} = 186 - 412R_S$. The largest member, S XXVI Albiorix, is also the object with the lowest semi-major axis among the group, $a_{\text{avg}} = 271R_S$. This provides evidence that any fragmentation must have happened after any substantial gas envelope dissipated. All the members have high average eccentricity, $e_{\text{avg}} = 0.46 - 0.53$, which together with the tight clustering in inclination, strongly suggest that the four objects have a common origin.

We observed three of the four known members of this family and find, contrary to our earlier work (Grav *et al.*, 2003), that the family does not have homogenous colors (see Fig. 1). The new observations show that Albiorix has a significant steeper spectral slope, at $S'_2 = 12.5 \pm 0.4\%$, compared to S XXI Tarvos and S XXVIII Erriapo, with slopes of $S'_2 = 5.4 \pm 1.0\%$ and $S'_2 = 5.1 \pm 0.7\%$ respectively. This results does not support the hypothesis that the three objects are fragments of a larger progenitor. However, a closer look at the individual observations show that Albiorix has a large span of different spectral slopes, from $S'_2 = 5.3 \pm 0.8\%$ in the observations on January 6th, 2005, to $S'_2 = 14.9 \pm 0.5\%$ in the observation on April 13th, 2005. It is thus evident that the colors of Albiorix varies over its surface. Figure 4 shows the reflectance spectra of these three objects. It is easily seen that Tarvos and Erriapo have linear slopes to the 1σ confidence level, while Albiorix has a linear slope at a $3 - \sigma$ (lower) confidence level in the January 2005 observations. The April 2005 observation, however, is significantly non-linear with a very steep slope from the B- to the R-filter ($S'_{2(B-R)} = 19.0 \pm 0.7$) and a shallower R- to I-filter slope ($S'_{2(R-I)} = 5.6 \pm 1.2$). The two new observations of Albiorix reported in this paper are displayed separately in Fig. 4 clearly showing their differences. The slope of the January 2005 observation of Albiorix is remarkable similar to the slopes of both Tarvos and Erriapo. We thus hypothesize that Tarvos and Erriapo are the largest fragments from an impact on Albiorix, leaving a less red crater. The phase curves of this family further supports the notion that the objects are indeed of similar origin (see Fig. 8). Their phase curves are all fairly shallow, with a weighted mean phase slope of $G = 0.39$. The Gallic irregular satellites thus span the range for main belt asteroids ($G \sim 0.1 - 0.5$; *Bowell et al.*, 1989). Additional observations are needed to further constrain the phase curve fits for both Tarvos and Erriapo.

The question is now whether a cratering event is possible for Gallic satellites. We find that a dispersion velocity of ~ 90 m/s needed to displace both the two smaller satellites to their current orbits from that of Albiorix. Such an impact could have been the result of ~ 1.25 km planetesimal hitting with a collisional velocity of 4.79 km/s. The impact would be just sub-catastrophic, excavating a crater with a radius of ~ 12 km. Such a collision has a 50% probability of happening for a disk with $M_{\text{disk}} \gtrsim 50 - 100M_{\oplus}$, depending on the size distribution of planetesimals. While this is a substantial disk, the many large craters on Phoebe is further evidence of such a massive disk (*Porco et al.*, 2005).

It is important to note that *Ćuk and Burns (2004b)* found that the primordial dynamical distribution of this family of objects may have been significantly altered when the Great Inequality resonance ($\xi = 5\lambda_S - 2\lambda_J - 2\varpi - \varpi_S$) swept through the region during the migration of Jupiter and Saturn to their present configuration. This of course complicates our understanding of this family, and as mentioned by *Ćuk and Burns (2004b)* more study of the impact of this resonance on the Gallic family is indeed needed. In particular, it would significantly help our understanding of the evolution of the irregular satellites to know whether this resonance favors the phase space currently inhabited by the Gallic family for capture. If so, it could be that the Gallic cluster is populated by objects that during the sweeping of the Great Inequality resonance during planet migration was moved into the cluster from a larger region of the surrounding phase space. Such a study, coupled with the determination of any variations in color on the surface of Albiorix, would indicate whether these objects are indeed fragments from a cratering event on Albiorix, rather than the products of

individual captures.

3.2 The Inuit Family

The Inuit cluster is centered around $\sim 45^\circ$ inclination and have four known members. Their semi-major axes are more spread out, $a_{\text{avg}} = 186 - 297R_S$, than the Gallic cluster, but is still fairly clustered compared to the large spread of all the Saturnian irregular satellites. The eccentricities are also clustered, with average values $e_{\text{avg}} = 0.29 - 0.35$. This points to a common origin for the members of this cluster.

For the Inuit family we observed all the four known members and the broadband colors and spectra are shown in Fig. 2 and 5, respectively. The results show that this cluster is very interesting, showing both dynamical (through the interaction of its members with different resonances) and physical diversity. All the four members of this dynamical family have been reported as possibly caught in resonances (Carruba *et al.*, 2002; Cuk *et al.*, 2002; Nesvorný *et al.*, 2003). In order to confirm this we used updated orbits from observations collected by the MPC between 2000-2006 (Marsden, personal communications), and numerically integrated the four objects using a Wisdom-Holman symplectic mapping scheme (Wisdom and Holman, 1991) for 10^7 years. The results confirm that S XXII Ijiraq and S XXIV Kiviuq are found to reside in the Kozai resonance, while S XXIX Siarnaq resides in the secular resonance $g - g_S = 0$, where g and g_S are the satellite and saturnian apsidal frequencies. As reported by Nesvorný *et al.* (2003), we also find that S XX Paaliaq does not seem to be associated with the $g - g_S = 0$ secular resonance.

3.2.1 S XX Paaliaq, S XXIV Kiviuq and S XXIX Siarnaq

The colors of the three satellites, Siarnaq, Paaliaq and Kiviuq, are very similar with a spectral slope range of $S'_2 \sim 10.0 - 13.2$. Paaliaq has a somewhat shallower slope than the two others, but also has the largest uncertainties of the three. The colors are very similar, with matching colors values in $B-V$, $V-R$ and $V-I$ at the $1-$, $2-$ and $3-\sigma$ levels, respectively. All three objects also test positive for the $0.7\mu\text{m}$ -feature, based on the method proposed by Vilas (1994). The reflectance spectra of these three objects are shown in Fig. 5 and the similarity is easily seen. All the color determinations of these three objects given in this paper is found to have linear slopes at a 2σ confidence level.

When comparing the phase curve slope parameter, G , of the Inuit cluster it is seen that both Paaliaq and Ijiraq have steeper phase curves than Siarnaq and Kiviuq. The fits for Ijiraq and Kiviuq is poor, however, due to only having two accurate photometric measurements each. The phase curve parameter derived for Siarnaq, $G = 0.27 \pm 0.04$, is lower than reported in Bauer *et al.* (2006), but the two values are within the 1σ confidence level of each other. The new value puts Siarnaq in the mid-range for main belt asteroids ($G \sim 0.1 - 0.5$; Bowell *et al.*, 1989), but higher than the usual values for C-, P- and D-type asteroids ($G \sim 0.09 \pm 0.09$; Harris *et al.*, 1989). The opposition surge of ~ 0.2 magnitudes seen in Siarnaq by Bauer *et al.* (2006) is not as narrow in our new fit. In fact none of the irregular satellites observed show any strong opposition surge, consistent with a high albedo surface (Tholen and Tedesco, 1994).

3.2.2 S XXII Ijiraq

Ijiraq is distinctly different from the three other members of this dynamical family. Its colors are moderately redder than the others and it does not show any indication of the $0.7\mu\text{m}$ -feature. The moderately red color found for Ijiraq does not, to our knowledge, appear anywhere in the inner solar system, indicating that its origin is the outer solar system where this color is common. The steep

phase curve slope further support the outer solar system as an origin for Ijiraq. With a phase curve parameter of $G = -0.14 \pm 0.22$ it is very similar to the phase curves of the Centaur population ($G \sim -0.13 - 0.04$; Bauer *et al.*, 2003, 2006; Rousselot *et al.*, 2005).

3.3 The Retrograde Satellites

There are currently 26 known retrograde Saturnian irregular satellites and they show dramatic dynamical and physical variety. The average semi-major axes of these satellites span the range from $213R_S$ to $412R_S$ and they have average inclinations varying from 138° to 176° . Even the average eccentricities show large variety from the low average eccentricity of S XXIII Suttungr, $e_{\text{avg}} = 0.115$, to the highly eccentric S/2004 S18, $e_{\text{avg}} = 0.501$. The retrogrades are thus unlikely be the result of a single capture and subsequent fragmentation. However, it is possible there exist smaller family clusters among the retrograde Saturnian irregular satellites, and using dynamical studies together with the photometric colors and phase curves reported in this paper will make searching for such families possible. The colors of the 5 retrograde irregular satellites that have been observed in this paper are shown in Fig. 3, together with the colors of Phoebe and Ymir (Grav *et al.*, 2003).

3.3.1 S XIX Ymir, S XXIII Suttungr, S XXX Thrymr

Comparing the results to earlier observations from Grav *et al.* (2003) reveals some interesting results. Interestingly the B-V color for Ymir has been found to have changed significantly. Furthermore, recent observations by the authors to determine the rotational light curve for Ymir show that the object has a significant peak-to-peak amplitude of ~ 0.3 magnitudes. It thus seems likely that Ymir has significant surface variegation and most likely an irregular shape. The result from Grav *et al.* (2003) is similar to the colors and slopes of Suttungr and Thrymr found in this paper, both which have similar mean orbital elements to Ymir (see table 5). This leads us to speculate whether Suttungr and Thrymr might be fragments broken off Ymir during an impact event. The fact that the two fragments have shallow slope (indicating that their surfaces have not been reddened by exposure to cosmic rays) might be an indication that the impact may have been fairly recent.

The broadband colors of Suttungr and Thrymr show a sharp dip in the V filter, as can be seen in Fig. 6. While the slope of Thrymr barely can be fitted to a straight line at the 3σ confidence level giving $S'_2 = 1.1 \pm 0.8$, the dip in the reflectance spectra of Suttungr is significant even at the 3σ confidence level when using the best fit. A similar, but less significant trend is also seen in the observation of Ymir reported in Grav *et al.* (2003). We thus believe that the feature is indeed real, but confirmation of this feature is needed either through more accurate broadband photometry or low-resolution spectra. The LRIS B- and V-filters have a central wavelength of $\lambda_c = 436.9$ nm and $\lambda_c = 543.7$ nm with fwhm values of $\Delta\lambda = 88$ nm and $\Delta\lambda = 92$ nm, respectively. It is therefore possible that what is seen is a positive feature at wavelengths just below 400nm that increases the flux in the B-filter, rather than an absorption feature in the V filter. Such behavior is known among some objects in the cometary population (such as P/Tuttle and IRAS-Araki-Alcock; Tholen and Zellner, 1984) and the jovian irregular satellites J XI Carme (Luu, 1991). Spectra of H_2O -, C_2O - and NH_3 -frost all show a significant upturn in the U-filter (Hapke *et al.*, 1981). All of these types of frost have distinctive features in the near-infrared, thus Ymir, Thrymr and Suttungr are prime candidates for searching for these features. While near-infrared spectra will be nearly impossible to do on these three faint objects, careful preparation might allow for the collection of JHK photometry for these two satellites. Photometric observations in the U-filter would also be very helpful to confirm the possible upturn at low visible wavelengths.

The notion that these smaller bodies are fragments of Ymir is, however, put into question by a quick look at their orbital elements. Computing dispersion velocities based on Gauss equations we find that Thrymr, S/2006 S4 and S/2004 S8 can be explained with a dispersion velocity of $\delta V \sim 175$ m/s. Suttungr, however, needs a dispersion velocity of $\delta V > 300$ m/s, due to the large difference in eccentricity (from 0.338 to 0.115). These dispersion velocities are again significantly higher than what is expected from a fragmentation event (Benz and Asphaug, 1999; Pisani *et al.*, 1999; Michel *et al.*, 2002). Using the formalism from Nesvorný *et al.* (2004) and assuming that $\sim 10\%$ of the impact energy is used to disperse the resulting fragments we find that in order for the four fragments to be related to Ymir, the progenitor was impacted by a ~ 1.75 km large body. The resulting impact energy using the collisional velocity of 4.63 km/s (Nesvorný *et al.*, 2004) is actually on the same order of magnitude as the energy needed to fully disrupt the progenitor. While the dispersion velocity is high and needs explaining, the significant amplitude of Ymir and the similarities of the colors supports the hypothesis that these objects are indeed the fragments of a catastrophic disruption of a progenitor with a radius of ~ 17 km. Again using the Nesvorný *et al.* (2004) formalism such a collision has a probability greater than 50% for a protoplanetary disk masses $M_{\text{disk}} \gtrsim 120 - 160M_{\oplus}$, depending on the size distribution of the residual planetesimal disk.

While we have determined phase curve parameters for Ymir, Suttungr and Thrymr in this paper, it should be noted that all fits have problems. Both the fits of Suttungr and Thrymr are very poor, with only one accurate photometric observation each (reported in this paper) and a few measurements reported to the MPC (for which we have assumed an uncertainty of 0.25 magnitudes). Additional photometric observations of these two satellites at a variety of phase angles are necessary in order to better constrain their fits, and thereby allowing us to compare the results to the other irregular satellites. The phase curve fit for Ymir has a low formal error ($G = 0.01 \pm 0.06$), but caution has to be taken. Data collected by the authors, but still in early stages of reduction, show that the rotational light curve has a significant peak-to-peak amplitude. It is therefore surprising to find such a good fit for the phase curve parameters. However, since the determination of any rotational light curve for Ymir is still unconfirmed we stand by the current fit, while cautioning the reader.

Even with the poor fits it seems clear that Suttungr has a fairly shallow slope ($G = 0.68 \pm 0.46$) compared to the steep slope of Thrymr ($G = -0.22 \pm 0.39$). This would suggest that the two satellites may have different surface composition and are therefore unlikely to have a common origin. Furthermore, the phase curve for Ymir is also steep ($G = 0.01 \pm 0.06$). This together with the high dispersion velocity needed to move Suttungr to its present orbit from that of Ymir, we conclude that it is unlikely that these two objects have a common origin. It should be noted that the difference in slope between Thrymr and Suttungr has a significance level of only $P = 0.136$, making it clear that additional observations and study are essential in order to better understand any relationship between these objects.

3.3.2 The neutrally colored objects: S IX Phoebe and S XXV Mundilfari

Mundilfari is a small moon, $d \sim 8$ km, that has average orbital elements of $a = 308R_S$, $e_{\text{avg}} = 0.211$ and $i_{\text{avg}} = 167.0^\circ$. There exists at least two other satellites with similar orbital elements, S/2004 S17 ($320R_S, 0.181, 167.8^\circ$) and S/2004 S13 ($303R_S, 0.259, 168.8^\circ$) that may have the same origin as Mundilfari. It would be extremely interesting to get color photometry of these two faint satellites, as a similar slope to that of the larger Mundilfari would be strong evidence of a collisional family within the retrograde irregular satellites.

Mundilfari is found to have a neutral to blueish spectral slope, $S'_2 = -5.0 \pm 1.9$, which is linear at the 2σ confidence level. It is seen to have a very shallow feature in the V filter, similar to that

of Suttungr and Thrymr. Its colors are similar to the colors of Phoebe at the 2σ confidence level and the slope is linear at the 2σ confidence level. The similarity with Phoebe leads us to believe that Mundilfari might have Phoebe as its origin. A dispersion velocity of $\delta V \sim 450\text{m/s}$ is needed to disperse Mundilfari to its current position, assuming that it is a fragment from a cratering event on Phoebe (Grav *et al.*, 2003; Nesvorný *et al.*, 2003, 2004). Again assuming that $\sim 10\%$ of the impact energy is used in the dispersion of fragments and a collision velocity of 5.07 km/s (from Nesvorný *et al.*, 2004) the impacting body is 2 km in radius and would excavate a crater with a diameter of 24km . Images from the Cassini-Huygens space craft show that Phoebe is covered with craters ranging from 100km in diameter and down (Porco *et al.*, 2005). It should be noted that again the dispersion velocity is significantly higher than results from laboratory tests or hydrocode simulations.

Unfortunately, no other accurate photometric observations exist of Mundilfari. Thus an accurate phase curve can not be determined. Using the inaccurate photometric measurements reported with astrometry to the Minor Planet Center the phase curve is fitted with an essentially flat slope, but the accuracy of the fit makes any comparisons of little worth at this point. Additional observations of Mundilfari at both low and high phase angles are necessary to test whether it has the same phase curve parameter as Phoebe.

3.3.3 S XXVII Skathi

This satellite has a spectral slope of $S'_2 = 5.2 \pm 2.8$, which identifies it as a P-type surface. The slope is linear and appears featureless at the 1σ uncertainty level. Its colors is very similar to that of Ymir, but it's orbital parameters make any association with Ymir unlikely. It should be noted that Skathi is currently in the region of phase space where secular resonances might have significantly influenced it, but currently its longitude of perihelion, ϖ , is circulating in the direction of its orbital motion (Ćuk and Burns, 2004b). The relationship to the other irregular satellites in its vicinity, particularly S/2004 S19, remains uncertain. Further color photometric observations of the many new retrograde satellites are needed to further explore the existence of possible families, which would help constrain the number of captures needed to create the current distribution.

3.4 The lack of ultra red matter among the Saturnian irregular satellites

It is widely believed that the irregular satellites are captured bodies that were formed in the planetesimal solar disk independent of the planets. The color distribution of the Saturnian irregular satellites give little in suggestions for their source region, but non the less it is generally assumed that the irregular satellites (especially those of the outer planets) have an origin in the outer solar system, as evident by the density of Phoebe (Johnson and Lunine, 2005). Figure 11 shows the spectral distributions of possible source populations to the irregular satellites. The data for the main belt asteroids and trojans was collected using objects in the SDSS Moving Object Catalog with photometry with $\delta m < 0.05$ (Ivezic *et al.*, 2002). Values for the outer Solar System populations were computed from observations in Peixinho *et al.* (2004), Doressoundiram *et al.* (2005) and Sheppard and Trujillo (2006).

The distributions show that the irregular satellites of Saturn most likely have two sources, one in the main asteroid belt, and one in the outer Solar System. The distribution of the Saturnian irregular satellites is incompatible with both the Centaur, classic Kuiper belt (CKBOs) and Plutino populations, but is in fairly good agreement with the scattered disk population (SDOs; Doressoundiram *et al.*, 2005). The Centaur population also presents a possible source population if one assumes that the it consists of two separate population, one with slopes $0 - 15\%$ per 100nm and another

with slopes 15 – 30% per 100nm (Peixinho *et al.*, 2003). A better understanding of the processes behind the bimodal color distribution among the Centaurs is needed, however, to confidently present its less red population as a source region for the Saturnian irregular satellites. The high number of negative sloped, bluish sloped satellites in our sample is hard to explain from the distribution of Centaurs, SDOs or any other outer Solar system population, thus leading us to speculate that the inner population of Jovian trojans or main belt asteroids supply a fraction of the Saturnian irregular satellites. This is of course counteracted by the fact that Phoebe is one of these negative, bluish sloped objects. Further study is needed to understand this apparent contradiction.

However, if we assume that the origin of the Saturnian irregular satellites is in the outer Solar Systems it seems unlikely that no object with a surface covered by ultra red matter (URM) would be captured. No such ultra red matter is seen among the irregular satellites. Ijiraq, with a spectral slope of $S'_2 = 19.5 \pm 0.9$, is the highest sloped Saturnian irregular satellite. This is significant less than the URM covered surfaces, $S' = 25 - 50\%$ per 100 nm, found among both the Centaur and scattered disk populations. The same lack of URM is evident in the cometary nuclei, which are also believed to have their origins in the outer solar system (Jewitt, 2002). Using a collisional resurfacing model with triggered cometary activity Delsanti *et al.* (2004) concluded that most Centaurs should have very red colors, unless their collisional environment is significantly higher than expected. It is likely that the collisional environment of the Saturnian irregular satellites are higher than that of the Centaurs, due to the more constrained phase space they cover and the gravitational focusing of Saturn on heliocentric objects in its vicinity, thus creating less red surfaces due to increased cratering. A more thorough investigation on this issue is beyond the scope of this paper, but is very much needed.

Since the irregular satellites are believed to have been captured during the later epochs of giant planet formation, it is possible that the lack of URM is simply a result of the time scale of space weathering in the outer Solar System being longer than that of giant planet formation. This means that as objects were scattered inwards from the trans-Neptunian populations and captured by the planets, their surfaces were not yet heavily reddened by space weathering effects. A process is then, however, needed to halt further reddening for objects captured by the giant planets.

Jewitt (2002) hypothesize that the formation of ballistic or rubble mantles by sublimation on outer Solar System objects as they evolve into short period comets is a possible explanation for the lack of URM for the cometary nuclei. Since the Saturnian irregular satellites never enter the water sublimation zone no anticipation of global resurfacing by rubble mantles is expected (Jewitt, 2002). Ballistic mantles may form on the surfaces of the Saturnian irregular satellites if enough volatiles, in the form of CO_2 or other supervolatiles, are exposed near their surfaces. Resurfacing through a ballistic mantle of debris, resulting in a more neutrally colored surface, would then be created by outgassing from active portions of the satellite surfaces. No active outgassing is, however, known among the Saturnian irregular satellites.

While the low density of Phoebe points to the outer Solar System as the origin, it does not necessarily mean that it accreted in the trans-Neptunian populations. It is quite reasonable that the low density is due to the object originated in the protoplanetary disk between the planets. While the giant planets accreted most of the planetesimals in this region, a significant residual disk could survive for some time after the giant planets have built their cores. It is possible that some of these residuals could be captured into irregular satellites. No currently known objects is believed to have its origin in the region of the giant planets, so it is difficult to determine what the density of such a residual planetesimal would be. It seems, however, unlikely that the density would differ greatly from that of the more distant trans-Neptunian populations. Sheppard and Trujillo (2006) speculate that the irregular satellites, Jovian and Neptunian Trojans and the grey excited hot Kuiper belt objects may have a similar origin. Dynamical studies show that these population may be have been populated

by objects in the current giant planet domain that were dispersed, transported and trapped in their current locations during or just after the migration of the giant planets (Gomes, 2003; Morbidelli *et al.*, 2005).

3.5 The Norse satellites as the source of Iapetus dark side

Iapetus is unique among the satellites of Saturn in that the surface on the hemisphere facing in the direction of motion is very dark, on the order of a few percent, while the opposing hemisphere has an albedo roughly ten times greater. Cassini data (Buratti *et al.*, 2005) have shown that while the NIR spectra of the brightest terrains are consistent with a nearly three-quarters water-ice composition, the darker terrain's 1-5 μm spectra are consistent with water-ice surface concentrations on the order of a few percent at most. Ferric absorption bands have also been seen in the Cassini spectrum of dark material. Similar bands were reported earlier in ground-based spectra of the dark side of Iapetus, and in spectra of the darkest terrain on Hyperion (Vilas *et al.*, 1996; Jarvis *et al.*, 2000a), and were used to show a possible common origin for the dark material on the two satellites. The hypothesis of a similar origin for the dark material of Hyperion and Iapetus was further supported by the successful application of a two-component model (composed of icy and dark D-type asteroidal material) by Buratti *et al.* (2002) in the analysis of high-resolution ground-based optical spectra. Hence, it has been proposed that the dark material that coats the dark, low-albedo leading side of Iapetus might have an exogenous origin. Furthermore, its origin may be from among the retrograde irregular satellites (here termed the Norse satellites as they are named after the ice giants in Norse mythology; Soter, 1974; Cruikshank *et al.*, 1983; Buratti and Mosher, 1995; Vilas *et al.*, 1996; Owen *et al.*, 2001) and that the same source may possibly coat the surface of Hyperion to a lesser extent. The low-albedo surface of Iapetus has a spectral slope of $S'_2 \sim 7.2\%$ (Tholen and Zellner, 1983). Phoebe was the satellite originally proposed as the common source of the dark material, with Poynting-Robertson drag as the potential transport mechanism (Soter, 1974). However, the C-type spectra of this largest irregular satellite (Clark *et al.*, 2005) is not compatible with the theory that Phoebe is the direct source of the material (Buratti *et al.*, 2005). Some closer matches exist among the irregular satellites from the retrograde group in our color-photometry data. The best candidates for the source of this material thus far are Ymir and Skathi, which exhibit spectral slopes of 5-8 percent, but the future task remains to compare the material spectroscopically.

4 Conclusions

- The Saturnian irregular satellites show a surprising diversity in colors, ranging from neutrally colored Phoebe and Mundilfari, to the moderately red colors of Albiorix and Ijiraq.
- None of the observed satellites exhibit ultrared surfaces, as have been observed in the trans-Neptunian populations.
- The surface of Albiorix appears to be variegated (at a $> 3 - \sigma$ level). Two of the other Gallic family members we sampled have similar spectral slopes as one portion of Albiorix's surface terrain, and could possibly be products of a collision with the larger irregular satellite. A common origin is furthermore supported by their shared shallow phase curve behavior.
- We find a strong agreement in the spectral slope of three of the four Inuit family members we have sampled, possibly indicative of a common origin.

- The surface of Ymir also appears to be variegated and may be the parent body of Thrymr and Suttungr, broken apart due to a collision with a ~ 2 km body.
- Our retrograde sample of satellites show marked diversity. However, two members, Phoebe and Mundilfari, both show uniquely blue slopes, while dynamical arguments support the possibility that they too may have a common origin.

5 Acknowledgments

Based on observations obtained in program GN-2004B-Q-42 and GN-2005A-Q-33 at the Gemini Observatory, which is operated by the Association of Universities for Research in Astronomy, Inc., under a cooperative agreement with the NSF on behalf of the Gemini partnership: the National Science Foundation (United States), the Particle Physics and Astronomy Research Council (United Kingdom), the National Research Council (Canada), CONICYT (Chile), the Australian Research Council (Australia), CNPq (Brazil) and CONICET (Argentina). Some of the data presented herein were obtained at the W. M. Keck Observatory, which is operated as a scientific partnership among the California Institute of Technology, the University of California and the National Aeronautics and Space Administration. The Observatory was made possible by the generous financial support of the W. M. Keck Foundation. This work has been supported by grants NASA/JPL-RSA1264797 and NASA/JPL1270738.

References

- Bauer, J. M., T. Grav, B. J. Buratti, and M. D. Hicks 2006. The phase curve survey of the irregular saturnian satellites: A possible method of physical classification. *Icarus* **184**, 181–197.
- Bauer, J. M., K. J. Meech, Y. R. Fernández, J. Pittichova, O. R. Hainaut, H. Boehnhardt, and A. C. Delsanti 2003. Physical survey of 24 Centaurs with visible photometry. *Icarus* **166**, 195–211.
- Belskaya, I. N., J. L. Ortiz, P. Rousselot, V. Ivanova, G. Borisov, V. G. Shevchenko, and N. Peixinho 2006. Low phase angle effects in photometry of trans-neptunian objects: 20000 Varuna and 19308 (1996 TO₆₆). *Icarus* **184**, 277–284.
- Benz, W., and E. Asphaug 1999. Catastrophic Disruptions Revisited. *Icarus* **142**, 5–20.
- Bowell, E., B. Hapke, D. Domingue, K. Lumme, J. Peltoniemi, and A. W. Harris 1989. Application of photometric models to asteroids. In R. P. Binzel, T. Gehrels, and M. S. Matthews (Eds.), *Asteroids II*, pp. 524–556.
- Buratti, B. J., D. P. Cruikshank, R. H. Brown, R. N. Clark, J. M. Bauer, R. Jaumann, T. B. McCord, D. P. Simonelli, C. A. Hibbitts, G. B. Hansen, T. C. Owen, K. H. Baines, G. Bellucci, J.-P. Bibring, F. Capaccioni, P. Cerroni, A. Coradini, P. Drossart, V. Formisano, Y. Langevin, D. L. Matson, V. Mennella, R. M. Nelson, P. D. Nicholson, B. Sicardy, C. Sotin, T. L. Roush, K. Soderlund, and A. Muradyan 2005. Cassini Visual and Infrared Mapping Spectrometer Observations of Iapetus: Detection of CO₂. *ApJ* **622**, L149–L152.
- Buratti, B. J., M. D. Hicks, and A. Davies 2005. Spectrophotometry of the small satellites of Saturn and their relationship to Iapetus, Phoebe, and Hyperion. *Icarus* **175**, 490–495.
- Buratti, B. J., M. D. Hicks, K. A. Tryka, M. S. Sittig, and R. L. Newburn 2002. High-Resolution 0.33–0.92 μm Spectra of Iapetus, Hyperion, Phoebe, Rhea, Dione, and D-Type Asteroids: How Are They Related? *Icarus* **155**, 375–381.
- Buratti, B. J., and J. A. Mosher 1995. The dark side of Iapetus: Additional evidence for an exogenous origin. *Icarus* **115**, 219–227.
- Bus, S. J., and R. P. Binzel 2002. Phase II of the Small Main-Belt Asteroid Spectroscopic Survey A Feature-Based Taxonomy. *Icarus* **158**, 146–177.
- Carruba, V., J. A. Burns, P. D. Nicholson, M. Cuk, and R. A. Jacobson 2002. S2000S5 and S/2000S6: Saturnian moons trapped in the Kozai resonance. In *Bulletin of the American Astronomical Society*, pp. 902–+.
- Carvano, J. M., T. Mothé-Diniz, and D. Lazzaro 2003. Search for relations among a sample of 460 asteroids with featureless spectra. *Icarus* **161**, 356–382.
- Clark, R. N., R. H. Brown, R. Jaumann, D. P. Cruikshank, R. M. Nelson, B. J. Buratti, T. B. McCord, J. Lunine, K. H. Baines, G. Bellucci, J.-P. Bibring, F. Capaccioni, P. Cerroni, A. Coradini, V. Formisano, Y. Langevin, D. L. Matson, V. Mennella, P. D. Nicholson, B. Sicardy, C. Sotin, T. M. Hoefen, J. M. Curchin, G. Hansen, K. Hibbitts, and K.-D. Matz 2005. Compositional maps of Saturn’s moon Phoebe from imaging spectroscopy. *Nature* **435**, 66–69.

- Colombo, G., and F. A. Franklin 1971. On the formation of the outer satellite groups of Jupiter. *Icarus* **15**, 186–189.
- Cousins, A. W. J. 1978. VRI Photometry of E and F Region Stars [errata: 1978MNSSA..37...35C & 1980MNSSA..39...32C]. *Monthly Notes of the Astronomical Society of South Africa* **37**, 8–+.
- Cruikshank, D. P., J. F. Bell, M. J. Gaffey, R. H. Brown, R. Howell, C. Beerman, and M. Rognstad 1983. The dark side of Iapetus. *Icarus* **53**, 90–104.
- Ćuk, M., and J. A. Burns 2004a. Gas-drag-assisted capture of Himalia’s family. *Icarus* **167**, 369–381.
- Ćuk, M., and J. A. Burns 2004b. On the Secular Behavior of Irregular Satellites. *AJ* **128**, 2518–2541.
- Cuk, M., J. A. Burns, V. Carruba, P. D. Nicholson, and R. A. Jacobson 2002. New Secular Resonances Involving the Irregular Satellites of Saturn. In *Bulletin of the American Astronomical Society*, pp. 943–+.
- Ćuk, M., and B. J. Gladman 2006. Irregular satellite capture during planetary resonance passage. *Icarus* **183**, 362–372.
- Dahlgren, M., and C.-I. Lagerkvist 1995. A study of Hilda asteroids. I. CCD spectroscopy of Hilda asteroids. *A&A* **302**, 907–+.
- Davis, L. 1994. A reference guide to the iraf/daophot package.
- Delsanti, A., O. Hainaut, E. Jourdeuil, K. J. Meech, H. Boehnhardt, and L. Barrera 2004. Simultaneous visible-near IR photometric study of Kuiper Belt Object surfaces with the ESO/Very Large Telescopes. *A&A* **417**, 1145–1158.
- Doressoundiram, A., N. Peixinho, C. Doucet, O. Mousis, M. A. Barucci, J. M. Petit, and C. Veillet 2005. The Meudon Multicolor Survey (2MS) of Centaurs and trans-neptunian objects: extended dataset and status on the correlations reported. *Icarus* **174**, 90–104.
- Fukugita, M., T. Ichikawa, J. E. Gunn, M. Doi, K. Shimasaku, and D. P. Schneider 1996. The Sloan Digital Sky Survey Photometric System. *AJ* **111**, 1748–+.
- Gladman, B., J. J. Kavelaars, M. Holman, P. D. Nicholson, J. A. Burns, C. W. Hergenrother, J.-M. Petit, B. G. Marsden, R. Jacobson, W. Gray, and T. Grav 2001. Discovery of 12 satellites of Saturn exhibiting orbital clustering. *Nature* **412**, 163–166.
- Gomes, R. 2003. Planetary science: Conveyed to the Kuiper belt. *Nature* **426**, 393–395.
- Grav, T., M. J. Holman, B. J. Gladman, and K. Aksnes 2003. Photometric survey of the irregular satellites. *Icarus* **166**, 33–45.
- Hapke, B., E. Wells, J. Wagner, and W. Partlow 1981. Far-UV, visible, and near-IR reflectance spectra of frosts of H₂O, CO₂, NH₃ and SO₂. *Icarus* **47**, 361–367.
- Hardorp, J. 1980. The sun among the stars. III - Energy distributions of 16 northern G-type stars and the solar flux calibration. *A&A* **91**, 221–232.

- Harris, A. W., J. W. Young, E. Bowell, L. J. Martin, R. L. Millis, M. Poutanen, F. Scaltriti, V. Zappala, H. J. Schober, H. Debehogne, and K. W. Zeigler 1989. Photoelectric observations of asteroids 3, 24, 60, 261, and 863. *Icarus* **77**, 171–186.
- Hartmann, W. K., D. P. Cruikshank, and J. Degewij 1982. Remote comets and related bodies - VJHK colorimetry and surface materials. *Icarus* **52**, 377–408.
- Hartmann, W. K., D. J. Tholen, K. J. Meech, and D. P. Cruikshank 1990. 2060 Chiron - Colorimetry and cometary behavior. *Icarus* **83**, 1–15.
- Heppenheimer, T. A., and C. Porco 1977. New contributions to the problem of capture. *Icarus* **30**, 385–401.
- Ivezic, Z., M. Juric, R. H. Lupton, S. Tabachnik, and T. Quinn 2002. Asteroids Observed by The Sloan Digital Survey. In J. A. Tyson and S. Wolff (Eds.), *Survey and Other Telescope Technologies and Discoveries. Edited by Tyson, J. Anthony; Wolff, Sidney. Proceedings of the SPIE, Volume 4836, pp. 98-103 (2002).*, pp. 98–103.
- Jarvis, K. S., F. Vilas, S. M. Larson, and M. J. Gaffey 2000a. Are Hyperion and Phoebe Linked to Iapetus? *Icarus* **146**, 125–132.
- Jarvis, K. S., F. Vilas, S. M. Larson, and M. J. Gaffey 2000b. JVI Himalia: New compositional evidence and interpretations for the origin of Jupiter’s small satellites. *Icarus* **145**, 445–453.
- Jewitt, D., and J. Luu 1998. Optical-Infrared Spectral Diversity in the Kuiper Belt. *AJ* **115**, 1667–1670.
- Jewitt, D., and S. Sheppard 2005. Irregular Satellites in the Context of Planet Formation. *Space Science Reviews* **116**, 441–455.
- Jewitt, D., S. Sheppard, J. Kleyna, and B. G. Marsden 2005. New Satellites of Saturn. *IAU Circ.* **8523**, 1–+.
- Jewitt, D. C. 2002. From Kuiper Belt Object to Cometary Nucleus: The Missing Ultrared Matter. *AJ* **123**, 1039–1049.
- Johnson, H. L., and W. W. Morgan 1953. Fundamental stellar photometry for standards of spectral type on the revised system of the Yerkes spectral atlas. *ApJ* **117**, 313–+.
- Johnson, T. V., and J. I. Lunine 2005. Saturn’s moon Phoebe as a captured body from the outer Solar System. *Nature* **435**, 69–71.
- Jordi, K., E. K. Grebel, and K. Ammon 2006. Empirical color transformations between SDSS photometry and other photometric systems. *A&A* **460**, 339–347.
- Kaasalainen, S., J. Piironen, M. Kaasalainen, A. W. Harris, K. Muinonen, and A. Cellino 2003. Asteroid photometric and polarimetric phase curves: empirical interpretation. *Icarus* **161**, 34–46.
- Kenyon, S. J. 2002. Planet Formation in the Outer Solar System. *PASP* **114**, 265–283.
- Kenyon, S. J., and J. X. Luu 1998. Accretion in the Early Kuiper Belt. I. Coagulation and Velocity Evolution. *AJ* **115**, 2136–2160.

- Landolt, A. U. 1992. UBVRI photometric standard stars in the magnitude range 11.5-16.0 around the celestial equator. *AJ* **104**, 340–371.
- Luu, J. 1991. CCD photometry and spectroscopy of the outer Jovian satellites. *AJ* **102**, 1213–1225.
- Luu, J., and D. Jewitt 1996. Color Diversity Among the Centaurs and Kuiper Belt Objects. *AJ* **112**, 2310–+.
- Michel, P., P. Tanga, W. Benz, and D. C. Richardson 2002. Formation of Asteroid Families by Catastrophic Disruption: Simulations with Fragmentation and Gravitational Reaccumulation. *Icarus* **160**, 10–23.
- Morbidelli, A., H. F. Levison, K. Tsiganis, and R. Gomes 2005. Chaotic capture of Jupiter’s Trojan asteroids in the early Solar System. *Nature* **435**, 462–465.
- Nesvorný, D., J. L. A. Alvarellos, L. Dones, and H. F. Levison 2003. Orbital and Collisional Evolution of the Irregular Satellites. *AJ* **126**, 398–429.
- Nesvorný, D., C. Beaugé, and L. Dones 2004. Collisional Origin of Families of Irregular Satellites. *AJ* **127**, 1768–1783.
- Owen, T. C., D. P. Cruikshank, C. M. Dalle Ore, T. R. Geballe, T. L. Roush, C. de Bergh, R. Meier, Y. J. Pendleton, and B. N. Khare 2001. Decoding the Domino: The Dark Side of Iapetus. *Icarus* **149**, 160–172.
- Peixinho, N., H. Boehnhardt, I. Belskaya, A. Doressoundiram, M. A. Barucci, and A. Delsanti 2004. ESO large program on Centaurs and TNOs: visible colors-final results. *Icarus* **170**, 153–166.
- Peixinho, N., A. Doressoundiram, A. Delsanti, H. Boehnhardt, M. A. Barucci, and I. Belskaya 2003. Reopening the TNOs color controversy: Centaurs bimodality and TNOs unimodality. *A&A* **410**, L29–L32.
- Pisani, E., A. dell’Oro, and P. Paolicchi 1999. Puzzling Asteroid Families. *Icarus* **142**, 78–88.
- Pollack, J. B., J. A. Burns, and M. E. Tauber 1979. Gas drag in primordial circumplanetary envelopes - A mechanism for satellite capture. *Icarus* **37**, 587–611.
- Porco, C. C., E. Baker, J. Barbara, K. Beurle, A. Brahic, J. A. Burns, S. Charnoz, N. Cooper, D. D. Dawson, A. D. Del Genio, T. Denk, L. Dones, U. Dyudina, M. W. Evans, B. Giese, K. Grazier, P. Helfenstein, A. P. Ingersoll, R. A. Jacobson, T. V. Johnson, A. McEwen, C. D. Murray, G. Neukum, W. M. Owen, J. Perry, T. Roatsch, J. Spitale, S. Squyres, P. C. Thomas, M. Tiscareno, E. Turtle, A. R. Vasavada, J. Veverka, R. Wagner, and R. West 2005. Cassini Imaging Science: Initial Results on Phoebe and Iapetus. *Science* **307**, 1237–1242.
- Rousselot, P., J.-M. Petit, F. Poulet, and A. Sergeev 2005. Photometric study of Centaur (60558) 2000 EC₉₈ and trans-neptunian object (55637) 2002 UX₂₅ at different phase angles. *Icarus* **176**, 478–491.
- Sheppard, S. S., B. Gladman, and B. G. Marsden 2003. Satellites of Jupiter and Saturn. *IAU Circ.* **8116**, 1–+.

- Sheppard, S. S., D. C. Jewitt, J. Kleyna, and B. G. Marsden 2006. Satellites of Saturn. *IAU Circ.* **8727**, 1–+.
- Sheppard, S. S., and C. A. Trujillo 2006. A Thick Cloud of Neptune Trojans and Their Colors. *Science* **313**, 511–514.
- Simonelli, D. P., J. Kay, D. Adinolfi, J. Veverka, P. C. Thomas, and P. Helfenstein 1999. Phoebe: Albedo Map and Photometric Properties. *Icarus* **138**, 249–258.
- Soter, S. 1974. Brightness of iapetus. *Paper presented at IAU Colloq., 28, Cornell University.*
- Stern, S. A. 1995. Collisional Time Scales in the Kuiper Disk and Their Implications. *AJ* **110**, 856–+.
- Tholen, D. J., and E. F. Tedesco 1994. Pluto’s lightcurve: Results from four oppositions. *Icarus* **108**, 200–208.
- Tholen, D. J., and B. Zellner 1983. Eight-color photometry of Hyperion, Iapetus, and Phoebe. *Icarus* **53**, 341–347.
- Tholen, D. J., and B. Zellner 1984. Multicolor photometry of outer Jovian satellites. *Icarus* **58**, 246–253.
- Tody, D. 1993. IRAF in the Nineties. In R. J. Hanisch, R. J. V. Brissenden, and J. Barnes (Eds.), *ASP Conf. Ser. 52: Astronomical Data Analysis Software and Systems II*, pp. 173–+.
- Vilas, F. 1994. A cheaper, faster, better way to detect water of hydration on Solar System bodies. *Icarus* **111**, 456–467.
- Vilas, F., S. M. Larson, K. R. Stockstill, and M. J. Gaffey 1996. Unraveling the Zebra: Clues to the Iapetus Dark Material Composition. *Icarus* **124**, 262–267.
- Wisdom, J., and M. Holman 1991. Symplectic maps for the n-body problem. *AJ* **102**, 1528–1538.

6 Table Captions

Table 1: The time, instrument and geometry of the observations reported in this paper are shown. The solar, r , and observer, Δ , distance of the object is given in AU. The phase angle, α , is given in degrees. Notes a,b,c are given in order to better understand which observation of each object corresponds to values given in the subsequent tables.

Table 2: The color photometry with 1σ uncertainties are given. Notes a,b,c are given in order to better understand which observation of each object corresponds to values given in the other tables.

Table 3: The spectral slopes of the observations are given. All slopes are given in % per 100nm and all uncertainties are 1σ . Notes a,b,c are given in order to better understand which observation of each object corresponds to values given in the other tables.

Table 4: Physical parameters computed based on the available observations of the irregular satellites of Saturn. $H(1, 1, 0)$ and G values of Phoebe taken from Bauer *et al.* (2006). Mean radius of Phoebe is taken from Porco *et al.* (2005). 0.7μ -tests are based on formalism from Vilas (1994), with Y and N reflecting a positive and negative test, respectively.

Table 5: : Based on 10^7 y integrations using a Wisdom-Holman symplectic mapping scheme (Wisdom and Holman, 1991) based the current best fit orbits from the Minor Planet Center (Marsden, personal communications).

Table 1: Observational Geometry

Object	UT	r	Δ	α	Notes
Albiorix	LRIS-R&B 2005-Jan-06 10:40	8.9356	7.9602	0.8545	a
	GMOS-N 2005-Apr-13 05:40	8.9742	8.9755	6.4035	b
	ALFOSC 2001-Feb-18 21:30	9.1750	9.2304	6.1467	c, 1)
Tarvos	GMOS-N 2004-Nov-09 05:10	9.0066	8.6380	5.9780	
Erriapo	GMOS-N 2004-Nov-09 04:00	8.9398	8.5467	5.9653	
Siarnaq	LRIS-R&B 2005-Jan-06 11:47	8.9435	7.9686	0.8796	a
	GMOS-N 2005-Apr-15 06:30	8.9867	9.0185	6.3844	b
Paaliaq	LRIS-R&B 2005-Jan-06 10:10	9.0979	8.1222	0.8277	
Kiviuq	GMOS-N 2004-Nov-10 15:10	9.0183	8.6176	5.8912	a
	GMOS-N 2005-Apr-15 06:02	9.0199	9.0490	6.3622	b
Ijiraq	GMOS-N 2004-Nov-10 12:51	9.0374	8.6361	5.8771	
Ymir	LRIS-R&B 2005-Jan-06 08:10	9.1545	8.1811	0.9353	a
	GMOS-N 2005-Apr-13 06:04	9.1871	9.1817	6.2573	b
Skathi	LRIS-R&B 2005-Jan-06 08:50	9.1157	8.1428	0.9602	
Thrymr	LRIS-R&B 2005-Jan-06 09:10	8.8941	7.9190	0.8776	
Suttungr	LRIS-R&B 2005-Jan-06 09:36	8.9335	7.9585	0.8789	
Mundilfari	LRIS-R&B 2005-Jan-06 12:10	9.0969	8.1207	0.8015	

1) Re-reduction of observation reported in Grav *et al.* (2003)

Table 2: Color Photometry

Object	V	B-V	V-R	V-I	Notes
Albiorix	20.64 ± 0.01	0.80 ± 0.02	0.47 ± 0.02	0.76 ± 0.03	a
	21.32 ± 0.01	0.96 ± 0.02	0.52 ± 0.01	0.96 ± 0.02	b
	21.40 ± 0.07	0.79 ± 0.12	0.52 ± 0.07	1.06 ± 0.11	c,1)
Tarvos	23.01 ± 0.02	0.78 ± 0.04	0.43 ± 0.02	0.82 ± 0.03	
Erriapo	23.32 ± 0.01	0.71 ± 0.03	0.40 ± 0.02	0.86 ± 0.02	
Siarnaq	20.10 ± 0.01	0.87 ± 0.01	0.48 ± 0.01	1.03 ± 0.01	a
	20.72 ± 0.01	0.88 ± 0.01	0.49 ± 0.01	1.02 ± 0.01	b
Paaliaq	21.17 ± 0.02	0.86 ± 0.03	0.40 ± 0.03	0.92 ± 0.03	
Kiviuq	22.83 ± 0.01	0.86 ± 0.02	0.48 ± 0.01	0.98 ± 0.02	a
	22.63 ± 0.02	0.92 ± 0.04	0.50 ± 0.03	0.98 ± 0.03	b
Ijiraq	23.40 ± 0.01	1.05 ± 0.03	0.58 ± 0.02	1.09 ± 0.02	
Ymir	21.88 ± 0.02	0.80 ± 0.03	0.45 ± 0.02	0.89 ± 0.02	a
	22.43 ± 0.02	0.77 ± 0.04	0.41 ± 0.03	0.86 ± 0.04	b
Skathi	23.80 ± 0.05	0.72 ± 0.08	0.37 ± 0.06	0.88 ± 0.08	
Thrymr	23.70 ± 0.04	0.41 ± 0.06	0.59 ± 0.05	0.86 ± 0.07	
Suttungr	24.03 ± 0.04	0.47 ± 0.06	0.65 ± 0.05	0.78 ± 0.06	
Mundilfari	24.07 ± 0.03	0.58 ± 0.05	0.41 ± 0.04	0.52 ± 0.07	

1) Re-reduction of observation reported in Grav *et al.* (2003)

Table 3: Spectral Slopes

Object	S'_1	S'_2	$S'_{2(B-R)}$	$S'_{2(R-I)}$	Taxonomy	Notes
Albiorix	4.3 ± 0.9	5.3 ± 0.8	11.4 ± 1.5	-2.2 ± 1.3	P	a
	12.7 ± 0.6	14.9 ± 0.5	19.0 ± 0.7	5.6 ± 1.2	D	b
	11.1 ± 3.7	12.9 ± 4.1	12.7 ± 5.9	12.3 ± 9.5	D	c, 1)
		12.5 ± 0.4	17.3 ± 0.6	2.7 ± 1.0		Mean
Tarvos	5.3 ± 1.2	5.4 ± 1.0	8.1 ± 1.7	2.2 ± 2.0	P	
Erriapo	4.5 ± 0.9	5.1 ± 0.7	4.0 ± 1.7	6.1 ± 1.6	P	
Siarnaq	12.2 ± 0.3	13.2 ± 0.3	14.3 ± 0.6	12.3 ± 0.8	D	a
	11.8 ± 0.8	12.5 ± 0.9	9.8 ± 1.4	17.3 ± 2.0	D	b
		13.0 ± 0.3	13.5 ± 0.5	12.6 ± 0.7		Mean
Paaliaq	9.5 ± 1.2	10.0 ± 1.2	11.6 ± 1.9	9.5 ± 3.6	D	
Kiviuq	10.9 ± 0.6	11.4 ± 0.6	13.3 ± 1.0	8.9 ± 1.2	D	a
	12.2 ± 1.1	12.9 ± 1.2	17.1 ± 2.0	7.8 ± 2.8	D	b
		11.8 ± 0.6	14.1 ± 0.8	8.8 ± 1.1		Mean
Ijiraq	17.5 ± 0.8	19.5 ± 0.9	25.4 ± 1.4	11.2 ± 2.0	MR	
Ymir	7.4 ± 0.8	7.4 ± 0.7	9.9 ± 1.7	5.0 ± 2.0	D	a
	6.0 ± 1.3	6.1 ± 1.2	6.9 ± 2.1	5.6 ± 2.8	D	b
		8.1 ± 0.5	10.0 ± 0.9	5.0 ± 1.4		Mean
Skathi	5.3 ± 2.7	5.2 ± 2.8	2.8 ± 4.5	8.9 ± 6.0	P	
Thrymr	-2.6 ± 2.2	-3.0 ± 2.7			C	
Suttungr	-3.1 ± 2.0	-3.2 ± 2.2			C	
Mundilfari	-6.7 ± 2.0	-5.0 ± 1.9	-1.4 ± 3.1	-11.7 ± 4.0	C	
Phoebe	-2.6 ± 0.3	-2.5 ± 0.4	-2.5 ± 0.7	-2.8 ± 0.8	C	

1) Re-reduction of observation reported in Grav *et al.* (2003)

Table 4: Physical Parameters

Object	H(1,1,0)	G	Radius (km)	$0.7\mu\text{m}$ -test
Albiorix	10.87 ± 0.01	0.42 ± 0.06	~ 16	N 1.060 ± 0.005
Tarvos	12.61 ± 0.07	0.19 ± 0.15	~ 7	N 1.028 ± 0.006
Erriapo	13.27 ± 0.15	0.57 ± 0.34	~ 5	Y 0.974 ± 0.011
Siarnaq	10.24 ± 0.02	0.27 ± 0.04	~ 21	Y 0.937 ± 0.005
Paaliaq	11.27 ± 0.04	-0.04 ± 0.12	~ 13	Y 0.946 ± 0.016
Kiviuq	12.43 ± 0.16	0.27 ± 0.32	~ 8	Y 0.973 ± 0.002
Ijiraq	12.85 ± 0.12	-0.14 ± 0.22	~ 6	N 1.024 ± 0.012
Ymir	11.81 ± 0.02	0.01 ± 0.06	~ 10	N 0.997 ± 0.011
Skathi	14.04 ± 0.11	0.64 ± 0.52	~ 4	Y 0.910 ± 0.016
Thrymr	13.73 ± 0.08	-0.22 ± 0.30	~ 4	N 1.201 ± 0.027
Suttungr	14.08 ± 0.08	0.68 ± 0.46	~ 4	N 1.337 ± 0.041
Mundilfari	14.28 ± 0.08	0.95 ± 0.52	~ 3	N 1.146 ± 0.146
Phoebe	6.24 ± 0.01	0.02 ± 0.03	106.6 ± 1.1	N 1.023 ± 0.006

Table 5: Mean Orbital Elements

Object	a_{avg} [AU]	e_{avg}	i_{avg} [$^{\circ}$]	a_{min} [AU]	a_{max} [AU]	e_{min}	e_{max}	i_{min} [$^{\circ}$]	i_{max} [$^{\circ}$]
Gallic Satellites									
Albiorix	0.1092	0.4768	37.16	0.1075	0.1112	0.3256	0.6432	28.26	45.88
Tarvos	0.1217	0.5254	37.93	0.1189	0.1253	0.3580	0.7067	27.48	47.95
Erriapo	0.1170	0.4700	37.41	0.1148	0.1199	0.3156	0.6405	28.46	45.89
S/2004 S11	0.1141	0.4684	37.88	0.1118	0.1169	0.3075	0.6469	28.80	46.67
Inuit Satellites									
Siarnaq	0.1195	0.2962	47.74	0.1174	0.1220	0.0881	0.5565	40.35	54.31
Kiviuq	0.0756	0.3154	47.72	0.0753	0.0759	0.1358	0.5543	39.27	53.70
Ijiraq	0.0758	0.3047	48.08	0.0755	0.0762	0.1091	0.5659	39.12	54.03
Paaliaq	0.1002	0.3457	49.24	0.0992	0.1015	0.1101	0.6477	38.37	56.59
Retrograde Satellites									
S/2004 S18	0.1355	0.5006	138.42	0.1322	0.1398	0.2576	0.7809	126.06	152.71
Narvi	0.1289	0.4278	142.11	0.1266	0.1317	0.2272	0.6673	132.40	152.76
S/2004 S19	0.1226	0.3380	149.87	0.1206	0.1251	0.1989	0.4970	142.80	156.54
Skathi	0.1041	0.2737	151.93	0.1032	0.1053	0.1792	0.3772	146.73	157.03
S/2006 S2	0.1475	0.4773	153.37	0.1432	0.1534	0.3063	0.6599	143.48	161.98
S/2006 S1	0.1251	0.1442	155.88	0.1231	0.1273	0.0782	0.2218	151.82	159.77
S/2004 S9	0.1354	0.2442	156.21	0.1326	0.1390	0.1408	0.3635	150.98	161.01
S/2006 S3	0.1416	0.4511	156.75	0.1378	0.1466	0.3018	0.6080	148.39	163.91
S/2004 S15	0.1289	0.1464	158.69	0.1267	0.1315	0.0822	0.2225	154.72	162.51
S/2006 S8	0.1178	0.4642	159.23	0.1160	0.1203	0.3526	0.5816	152.09	165.70
S/2004 S12	0.1324	0.3289	164.62	0.1298	0.1360	0.2322	0.4325	159.70	169.09
S/2004 S16	0.1494	0.1401	164.72	0.1456	0.1540	0.0671	0.2240	160.90	168.39
S/2004 S14	0.1316	0.3709	165.04	0.1286	0.1356	0.2625	0.4885	159.53	169.78
S/2004 S10	0.1388	0.2546	166.53	0.1358	0.1427	0.1679	0.3486	162.35	170.34
S/2006 S6	0.1252	0.2175	162.79	0.1232	0.1277	0.1477	0.2960	158.76	166.61
Mundilfari	0.1243	0.2112	167.01	0.1224	0.1265	0.1527	0.2754	163.49	170.48
S/2006 S5	0.1532	0.1897	167.66	0.1490	0.1584	0.1049	0.2863	163.79	171.23
S/2004 S17	0.1293	0.1805	167.75	0.1270	0.1322	0.1197	0.2483	164.25	171.15
S/2004 S13	0.1226	0.2592	168.82	0.1207	0.1251	0.1901	0.3332	165.05	172.43
S/2004 S8	0.1661	0.2088	170.15	0.1602	0.1735	0.1061	0.3223	166.31	173.69
S/2006 S7	0.1519	0.4470	168.77	0.1463	0.1590	0.3074	0.5818	163.21	173.56
Ymir	0.1535	0.3376	172.86	0.1492	0.1592	0.2311	0.4454	169.23	176.48
S/2006 S4	0.1215	0.3267	174.24	0.1196	0.1240	0.2533	0.4013	171.09	177.53
Phoebe	0.0864	0.1635	174.91	0.0860	0.0869	0.1404	0.1883	172.52	177.92
Suttungr	0.1296	0.1152	175.69	0.1276	0.1319	0.0734	0.1612	173.34	178.78
Thrymr	0.1360	0.4659	175.24	0.1328	0.1402	0.3603	0.5672	171.97	178.95

7 Figure Captions

Figure 1: The observed colors for the Gallic family. Both the values from this work, as well as values from Buratti *et al.* (2005) and Grav *et al.* (2003) are plotted.

Figure 2: The observed colors for the Inuit family. Both the values from this work, as well as values from Buratti *et al.* (2005) and Grav *et al.* (2003) are plotted.

Figure 3: The observed colors for the retrograde Saturnian satellites. Both the values from this work, as well as values from Buratti *et al.* (2005) and Grav *et al.* (2003) are plotted.

Figure 4: The computed reflectance from the observations of the Gallic satellites in this paper are shown. 1σ uncertainties are shown for all observations and the spectra are offset to better compare their features. The S'_2 (dotted line), $S'_{2(B-R)}$ and $S'_{2(R-I)}$ (both dashed lines) are also shown.

Figure 5: The computed reflectance from the observations of the Inuit satellites in this paper are shown. The fitted values for S'_2 are plotted as dotted lines. 1σ uncertainties are shown for all observations and the spectra are offset to better compare their features.

Figure 6: The computed reflectance from the observations of the retrograde satellites. The reflectance of Ymir from Grav *et al.* (2003) is also shown. The dotted lines give the fitted S_2 spectral slope. 1σ uncertainties are shown for all observations and the spectra are offset to better compare their features.

Figure 7: The fitted spectral slope, S'_2 , of the Saturnian irregular satellites observed in this paper. Values for Phoebe is calculated from Grav *et al.* (2003). The slopes of Thrymr and Suttungr are fitted by excluding the V-filter observations.

Figure 8: The available observations are used to determine the IAU phase curve parameters, $H(1, 1, 0)$ and G , for the three Gallic satellites. The best fit (solid line) and error bars (gray lines) are given.

Figure 9: The available observations are used to determine the IAU phase curve parameters, $H(1, 1, 0)$ and G , for the three Inuit satellites. The best fit (solid line) and error bars (gray lines) are given.

Figure 10: The available observations are used to determine the IAU phase curve parameters, $H(1, 1, 0)$ and G , for the five Norse satellites. The best fit (solid line) and error bars (gray lines) are given.

Figure 11: The spectral slope distributions of several possible origin populations for the Saturnian irregular satellites compared to the distribution found for the irregular satellites in this paper. The ultrared material found in the Centaurs and KBOs does not seem to be present in the Saturnian irregular satellite population. However, the satellites do generally match the bluer component of the Centaurs. The main belt and Jovian Trojan population have been generated using the SDSS Moving Object Catalog (Ivezic *et al.*, 2002). The outer Solar System populations have been generated using data from Peixinho *et al.* (2004), Doressoundiram *et al.* (2005) and Sheppard and Trujillo (2006).

Colors of Gallic satellites

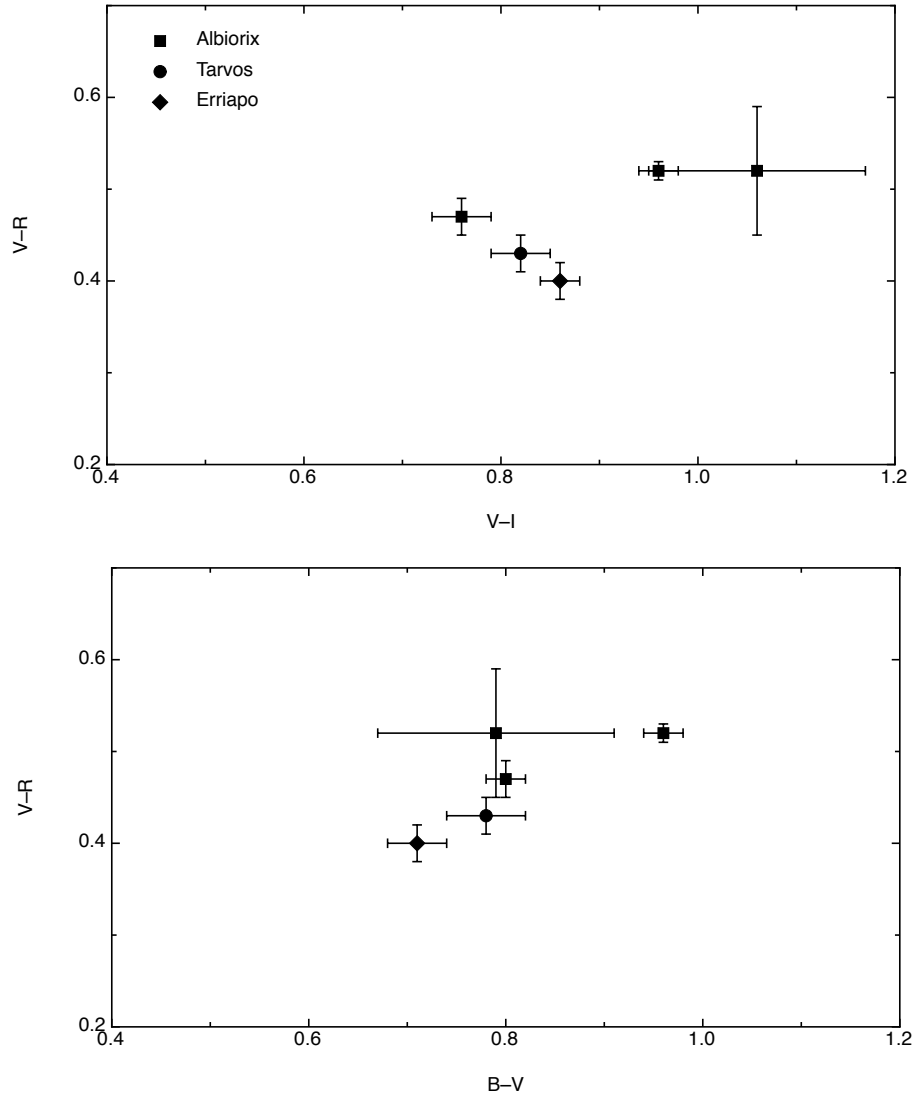


Figure 1:

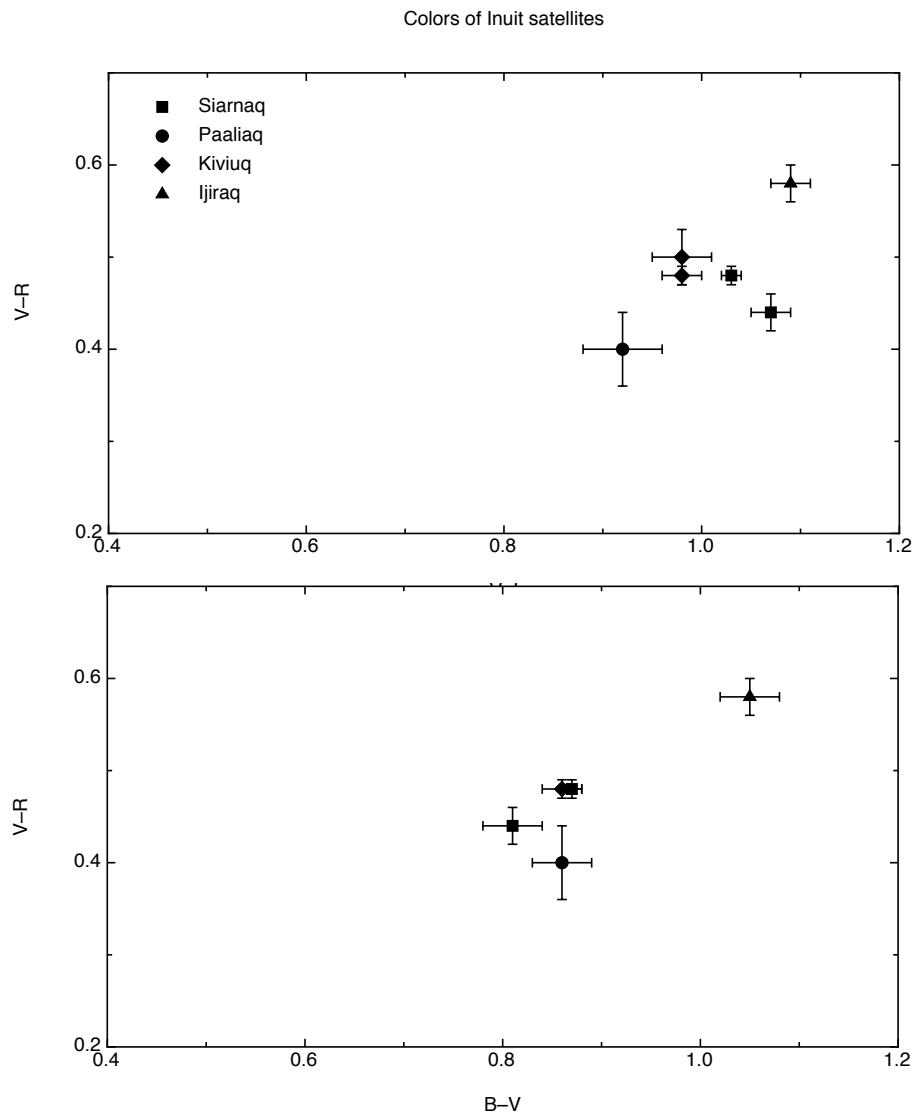


Figure 2:

Colors of the Norse satellites

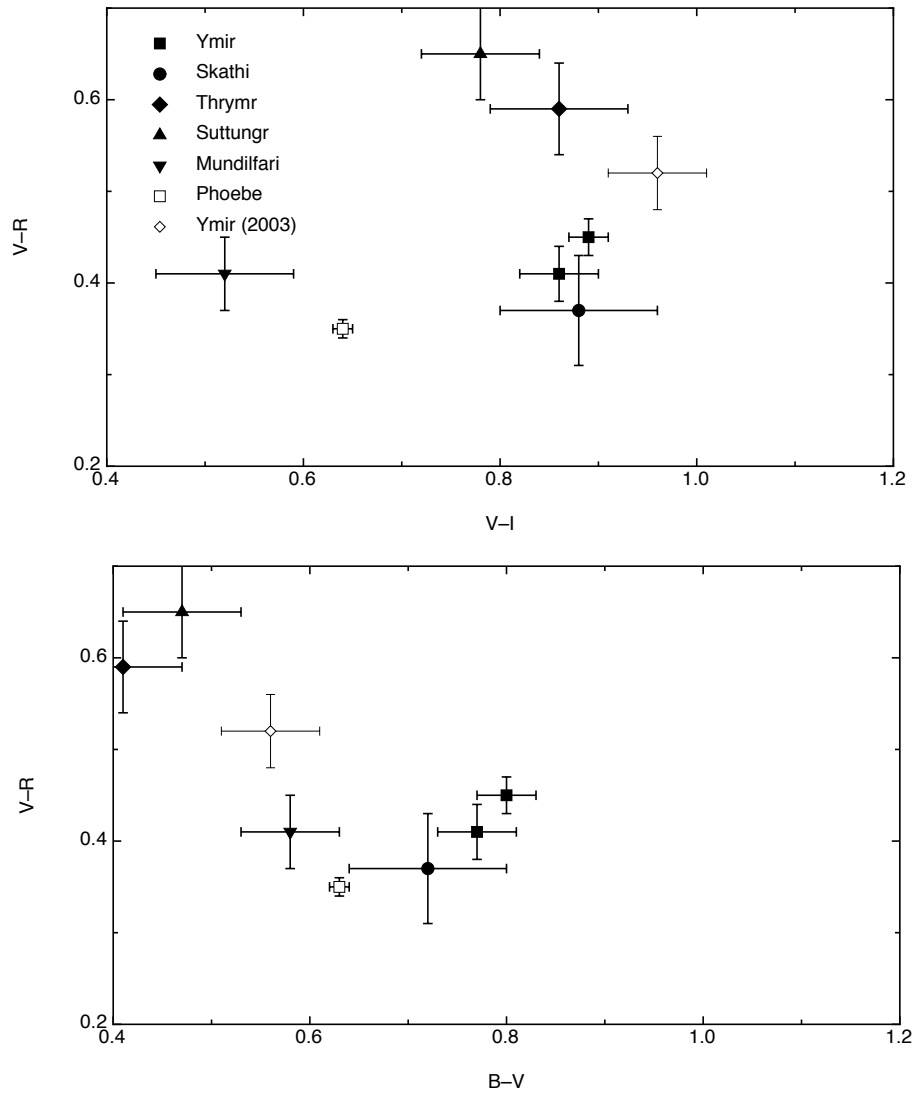


Figure 3:

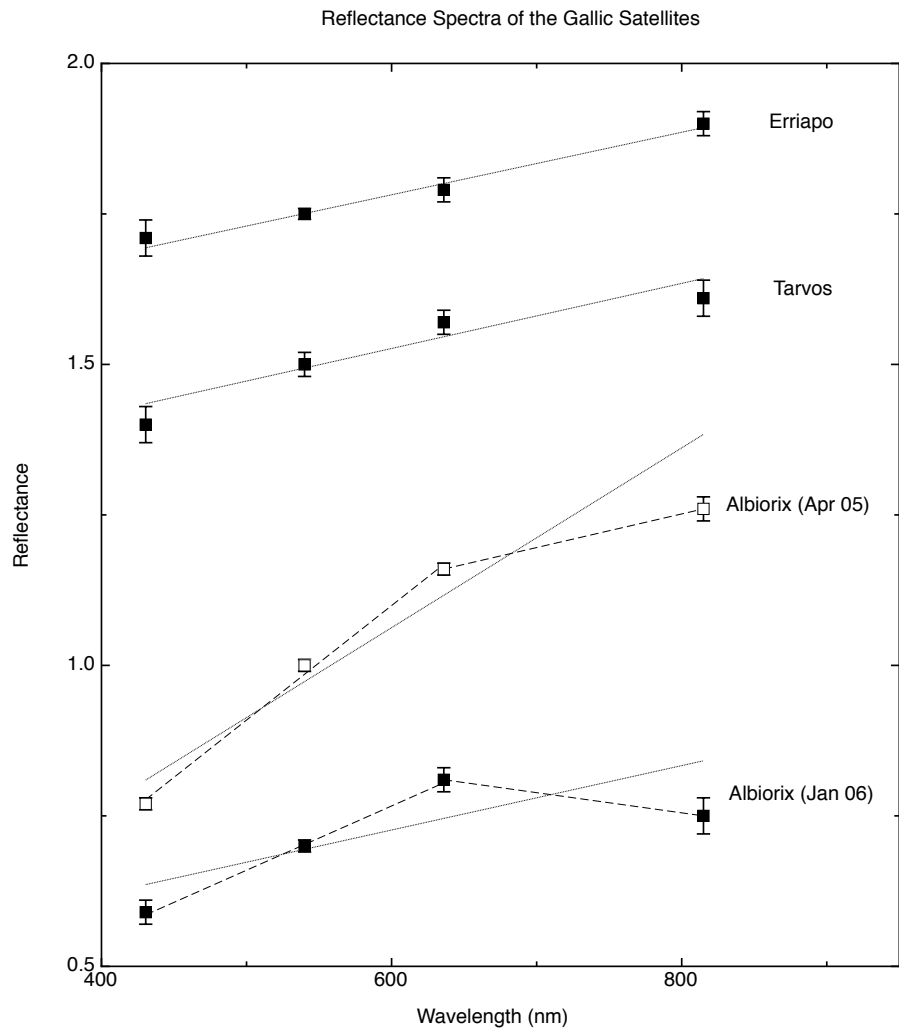


Figure 4:

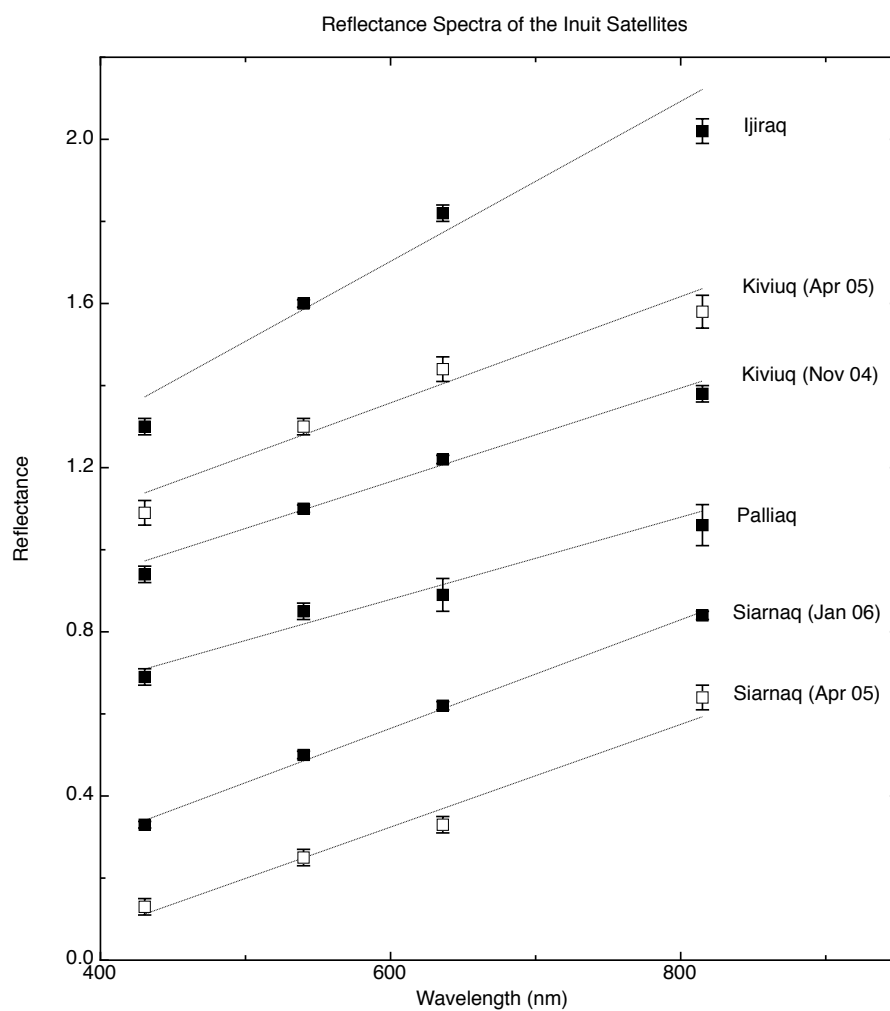


Figure 5:

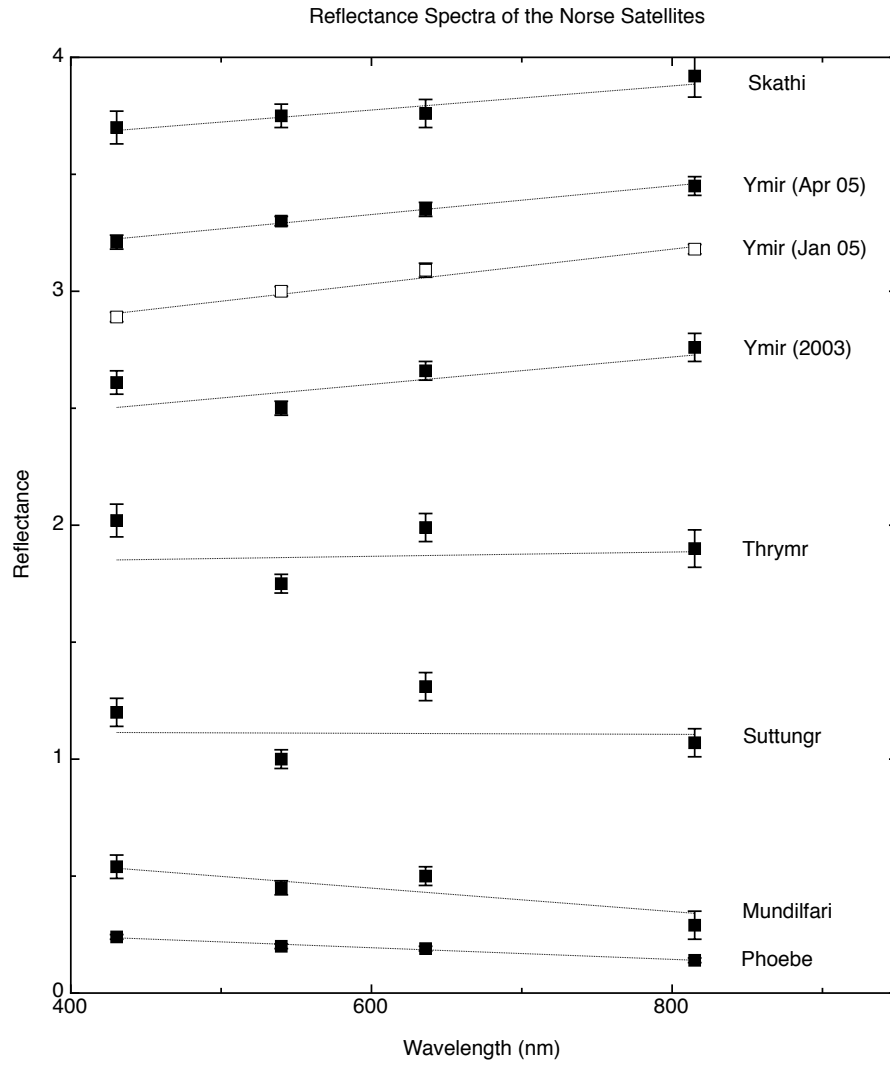


Figure 6:

Fitted spectral Slopes for the Saturnian Irregular Satellites

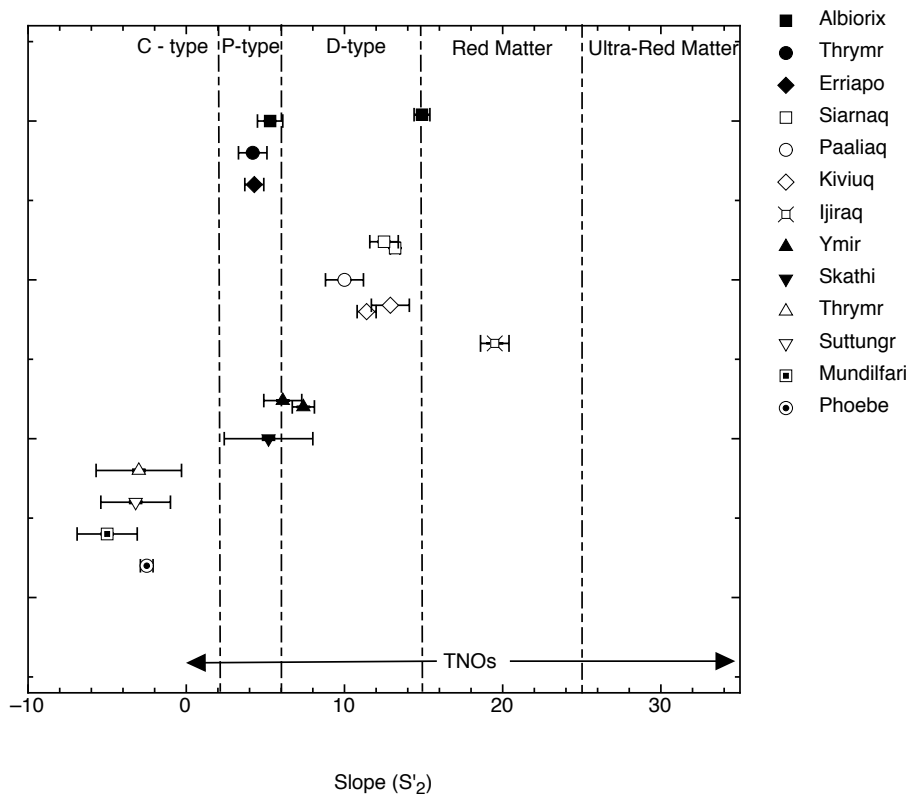


Figure 7:

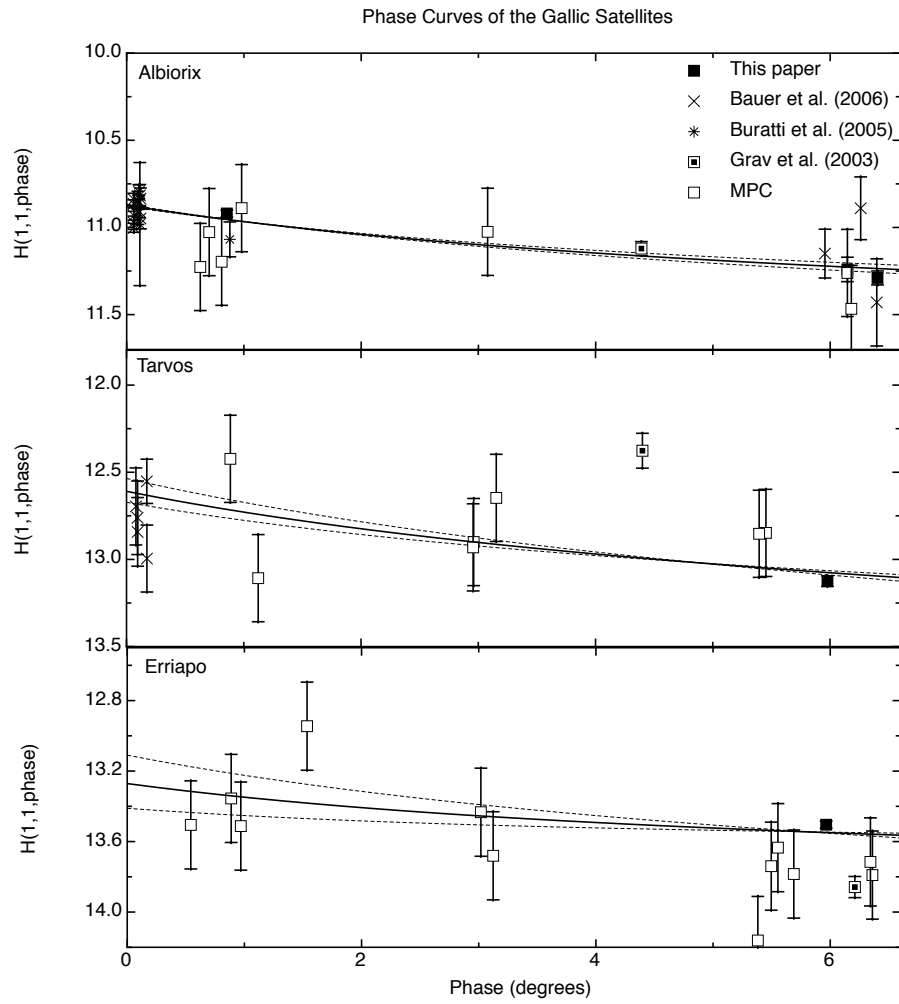


Figure 8:

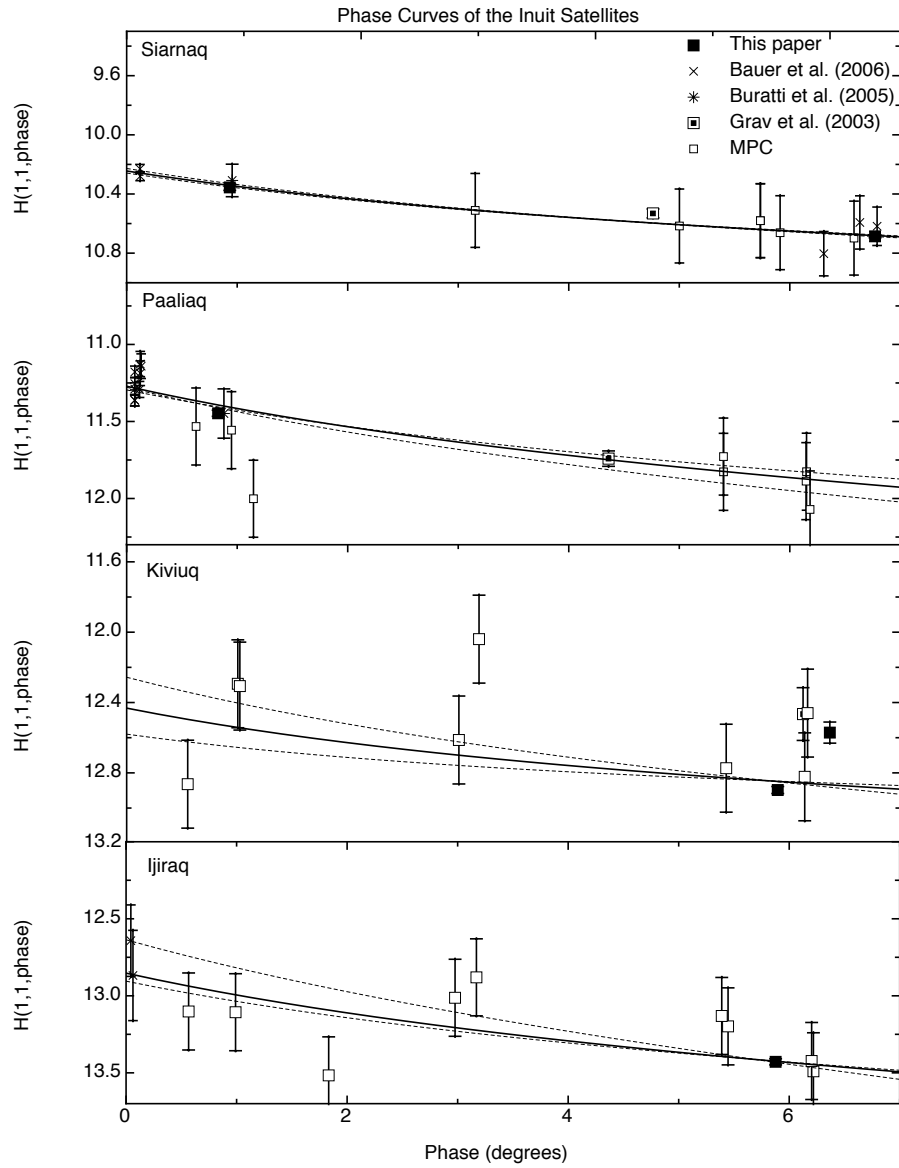


Figure 9:

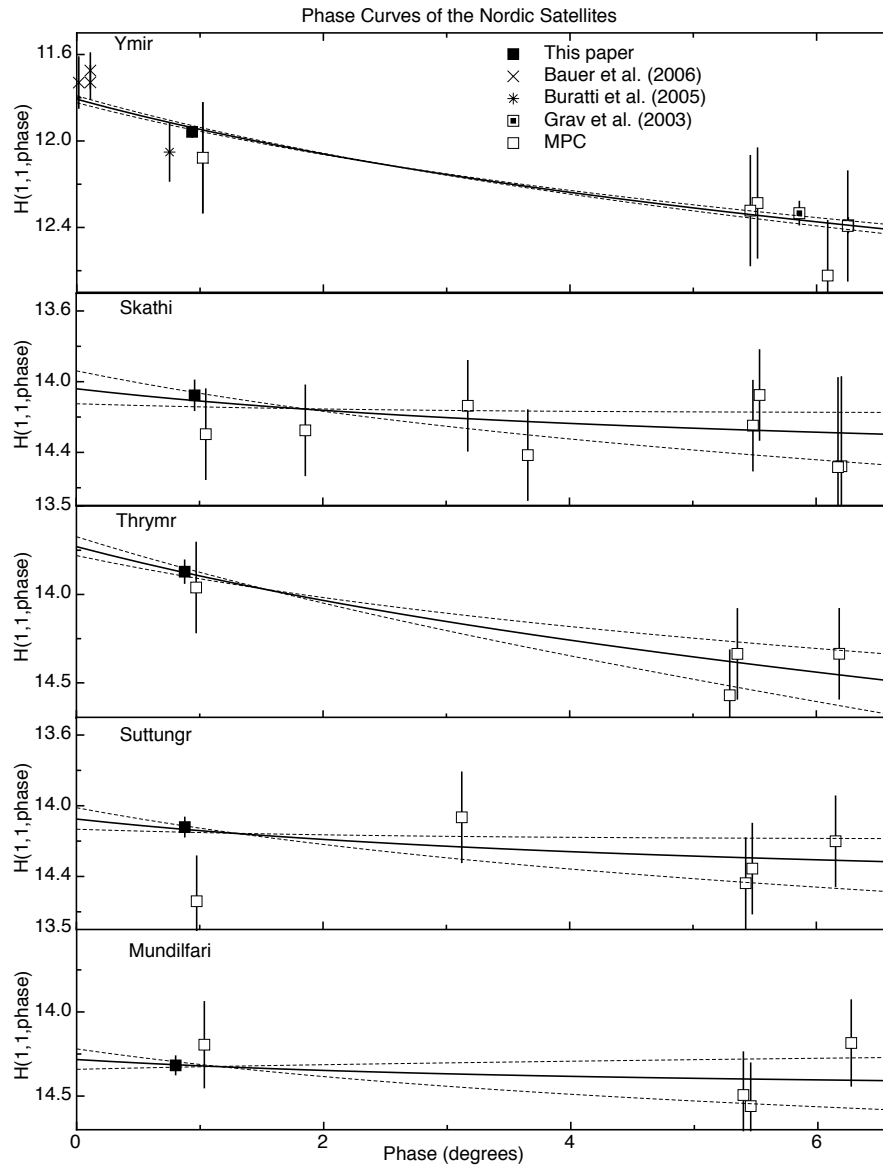


Figure 10:

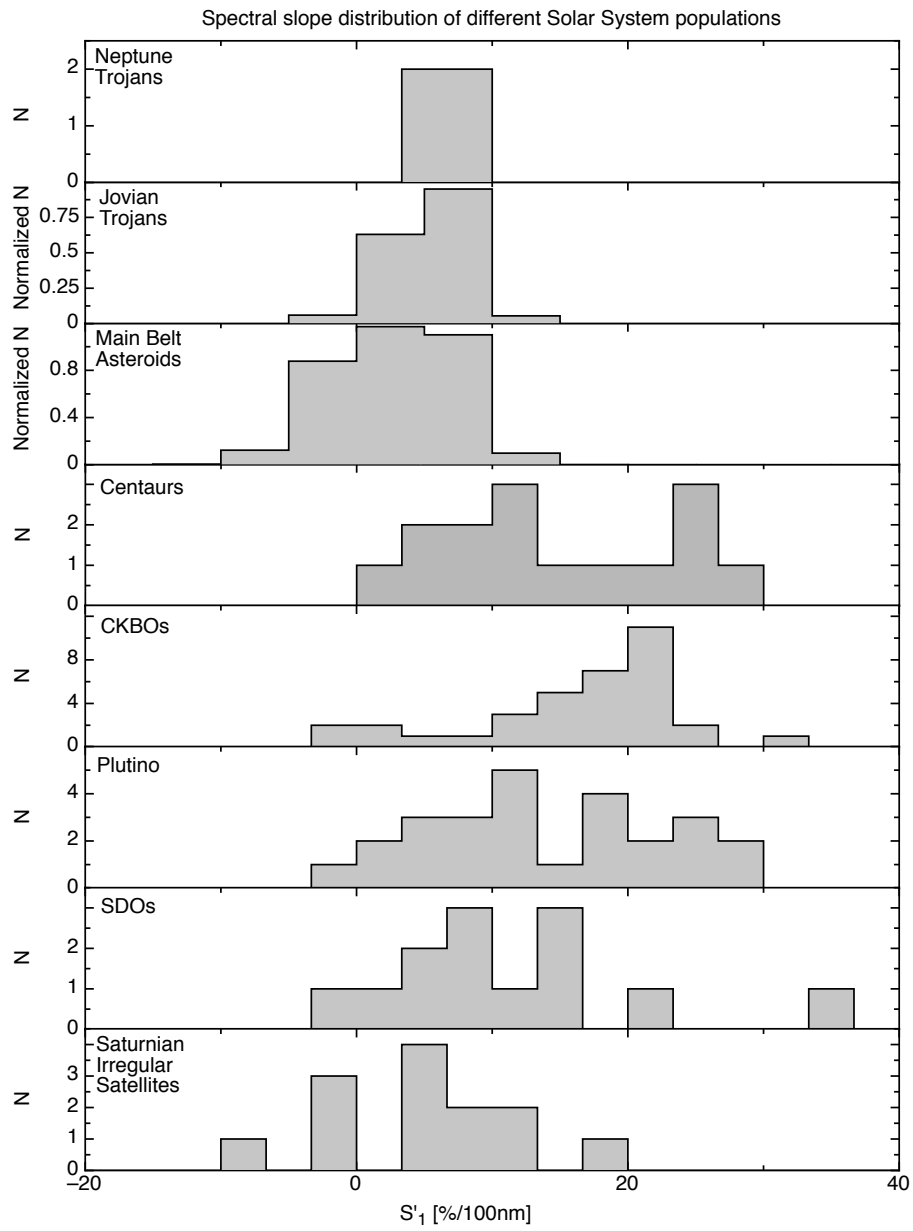


Figure 11: